ELSEVIER

Physica D 74 (1994) 197–253

PHYSICA D

Constants of motion for superconducting Josephson arrays

Shinya Watanabe, Steven H. Strogatz

Department of Mathematics, Massachusetts Institute of Technology, Cambridge, MA 02139, USA

Received 10 December 1993; revised 14 February 1994; accepted 14 February 1994
Communicated by H. Flaschka

Abstract

We show that series arrays of N identical overdamped Josephson junctions have extremely degenerate dynamics. In particular, we prove that such arrays have $N-3$ constants of motion for all $N \geq 3$. The analysis is based on a coordinate transformation that reduces the governing equations to an $(N-3)$-parameter family of low-dimensional systems. In the weak-coupling limit, the reduced equations can be analyzed completely. Either all solutions approach the synchronous state or they converge to a continuous family of incoherent oscillations, depending on a certain parameter value. At the transitional value of this parameter, the system becomes completely integrable. Then the phase space is foliated by invariant two-dimensional tori, for any $N \geq 3$. The infinite-N limit of the system is an integro-partial differential equation with rigorously low-dimensional dynamics. It supports solitons in the integrable case, and chaotic waves in the non-integrable case.

1. Introduction

Ever since the pioneering work of Fermi, Pasta and Ulam [1], computers have been used to shed light on the dynamics of many-body systems. Such numerical experiments have often led to serendipitous discoveries, sometimes with important ramifications. For instance, the observation of recurrence phenomena by Fermi et al. ultimately led to the discovery of solitons, the Toda lattice, and the theory of completely integrable systems.

In the past few years, some unexpected results have emerged from numerical experiments on series arrays of superconducting Josephson junctions. One of the goals of this paper is to bring these results to the attention of the dynamical systems community, especially those people interested in integrable systems, coupled oscillators, or condensed-matter physics. A second goal is to present a theory that explains much of what has been observed. Finally, we hope to encourage others to study these problems; the numerics suggest that our theory is incomplete, and that there is further structure waiting to be explained.

The relevant observations concern the following set of equations, obtained as the circuit equations for a broad class of Josephson arrays:

SSDI 0167-2789(94)00033-M

$$\dot{\phi}_j + \sin\phi_j + \dot{Q} = I_b, \quad j = 1,\ldots,N, \tag{1.1}$$

$$L\ddot{Q} + R\dot{Q} + C^{-1}Q = \frac{1}{N}\sum_{k=1}^{N}\dot{\phi}_k, \tag{1.2}$$

where the overdot denotes differentiation with respect to dimensionless time, and R, L, C and I_b are dimensionless circuit parameters.

As long as I_b is not too small, this system has certain periodic solutions known as splay states. Numerical experiments [2,3] show that the splay states have $N-2$ Floquet multipliers equal to $+1$, indicating an enormous degree of neutral stability. This peculiar result holds for a wide range of parameters and circuit configurations. Previous attempts to explain the neutral stability have used averaging theory [4] or continuum limits [5,6], followed by linear stability analysis. While instructive, these approaches are both approximate and local. Rigorous, global results have been lacking.

In this paper we explain the origin of the neutral stability by proving that the system has $N-3$ independent constants of motion. The constants are constructed explicitly, and their geometric meaning is discussed. The key to the analysis is a coordinate transformation that reduces the system to an $(N-3)$-parameter family of low-dimensional systems. Loosely speaking, this transformation plays a role akin to the inverse scattering transform for completely integrable Hamiltonian systems. The analogy is imperfect, however, because the Josephson arrays are typically neither Hamiltonian nor completely integrable — for many array configurations, the associated low-dimensional "reduced systems" can have limit cycles or chaotic solutions.

This paper is organized as follows. Section 2 presents background information on Josephson arrays and summarizes the relevant previous results. In particular, Section 2.4 lists three important numerical observations that have inspired the theoretical work.

The analysis begins in Section 3. We introduce a class of dynamical systems that includes Josephson arrays as a special case. Our transformation method shows that all systems of this class are explicitly reducible to systems with $N-3$ fewer variables. An immediate consequence is a bound on the dynamical complexity of Josephson arrays. For instance, the system (1.1, 1.2) is $(N+2)$-dimensional, yet its dynamics are now seen to be effectively five-dimensional.

Unfortunately, even after the reduction, the system is still difficult to analyze. To make further progress, Section 4 focuses on the averaged equations obtained in the limit of weakly coupled arrays. Now the reduced system can be analyzed completely. A Lyapunov function is obtained and used to prove that the system has a global attracting set. As a certain parameter is varied, the attracting set changes from a synchronous oscillation to a continuous family of incoherent oscillations. At the transitional value of the parameter, the system becomes *completely integrable*. Then almost all solutions are quasiperiodic on 2-tori, and are governed by a Hamiltonian system with one degree of freedom. For this special case, the Hamiltonian provides an extra constant of motion, bringing the total to $N-2$ conserved quantities. This structure underlies the invariant 2-tori detected in the early numerical experiments of Tsang et al. [7]. Of course, one has to be careful about extrapolating from the averaged system to the original, unaveraged Josephson array equations. Some features are destroyed by averaging; for instance, the array equations can have chaotic solutions, but the averaged system cannot. At the end of Section 4, we indicate which features of the averaged system hold in general.

Section 5 deals with reducible systems in the infinite-N limit. Here we have an unusual (but

pleasant) example of an infinite-dimensional system whose dynamics are guaranteed *a priori* to be effectively low-dimensional. The results and analysis in Sections 5.1 and 5.2 may be skipped on a first reading; they are similar to the finite-N case. The new results come in Sections 5.3 and 5.4. We investigate a completely integrable limit of the system, and show that it exhibits solitons. We present several numerical examples of soliton interactions as well as a non-integrable case where the waves are chaotic.

Section 6 highlights the limitations of the present study and discusses directions for future research. Appendix A shows the details of a calculation needed in Section 5.1. Appendix B presents a more algebraic and symmetric set of constants of motion for the completely integrable, finite-N case, and shows how they are related to the constants found earlier.

A preliminary report of our work on the integrable case has appeared elsewhere [8].

2. Background: Josephson junctions and arrays

Josephson junctions are superconducting devices that can generate voltage oscillations of high frequency, typically 10^{10}–10^{11} cycles per second. They offer exciting technological possibilities as parametric amplifiers, voltage standards, detectors, mixers, and fast switching devices for digital circuits. For an introduction to Josephson junctions and their applications, see [9–11].

2.1. Dynamics of a single junction

The dynamics of a Josephson junction is described in dimensionless form by

$$\beta\ddot{\phi} + \dot{\phi} + \sin\phi = I_b, \tag{2.1}$$

where $\phi(t)$ is the quantum mechanical phase difference across the junction, I_b is the dimensionless bias current and β is the McCumber parameter, a dimensionless measure of the capacitance of the junction [12,13]. We will assume throughout that I_b is time-independent, corresponding to a dc-current bias.

Note that (2.1) is precisely analogous to the equation governing a damped pendulum driven by a constant torque. This mechanical analog is often useful for visualizing the dynamics of Josephson junctions [9].

Depending on the size, geometry, and type of coupling used in the Josephson junction, the value of β can range from $\beta \approx 10^{-6}$ to much larger values, say $\beta \approx 10^{6}$. From now on, we will assume that all junctions have

$$\beta = 0, \tag{2.2}$$

the so-called *overdamped* limit. This limit is commonly studied in the Josephson literature [9–11], but since it is singular, it may cause some mathematical concern. Our justifications are: (1) For a single junction (or pendulum), the effects of the singular limit are confined to an initial transient. After a rapid relaxation onto a slow manifold, the dynamics for small β and zero β are similar. The same is probably true for arrays, although no results in this direction have been proven. (2) In any case, it is unclear how to make analytical progress for arrays of junctions with $\beta > 0$. The only available result is an existence proof for a particular kind of periodic solution [14].

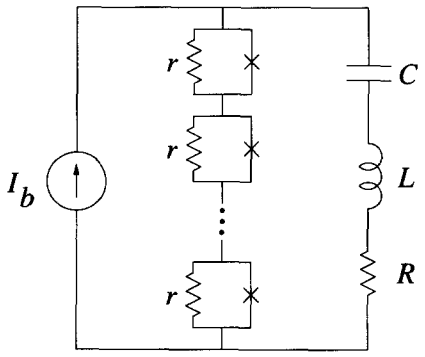

Fig. 1. A series array of Josephson junctions. The array is shunted by an *RLC* load to provide global coupling among the junctions.

2.2. Series arrays

Arrays of Josephson junctions are technologically interesting for their device applications [11,15, 16] and for their possible connection to high-temperature superconductors [17]. From a dynamical systems perspective, they offer intriguing examples of large systems of coupled nonlinear oscillators.

Arrays come in many different configurations: one-dimensional arrays connected in series or parallel, or two-dimensional arrays with various connectivities. We will restrict attention to the simplest case, in which N identical junctions are connected in series and driven by a constant bias current. Following [18,19], we also assume that a load is connected in parallel with the array; otherwise the junctions are not coupled.

Fig. 1 shows an array in which the load is a capacitor, inductor, and resistor in series. Notice that the individual junctions are drawn with an effective resistance r, but *without* an effective capacitance, consistent with our assumption that $\beta = 0$.

In dimensional form, the governing equations are

$$\frac{\hbar}{2er}\frac{d\phi_j}{dt} + I_c \sin\phi_j + \frac{dQ}{dt} = I_b, \quad j = 1,\ldots,N, \tag{2.3}$$

$$L\frac{d^2Q}{dt^2} + R\frac{dQ}{dt} + \frac{Q}{C} = \frac{\hbar}{2e}\sum_{k=1}^{N}\frac{d\phi_k}{dt}, \tag{2.4}$$

from Kirchhoff's current law and voltage law, respectively. Here $\hbar$ is Planck's constant divided by 2π, e is the charge on the electron, r is the junction resistance, $\phi_j(t)$ is the phase difference across junction j, I_c is the junction's critical current, $Q(t)$ is the charge on the load capacitor, I_b is the dc-bias current, and L, R, and C are the inductance, resistance, and capacitance of the load, respectively.

Note the permutation symmetry of the equations, as well as the presence of *global coupling* (or all-to-all coupling) in (2.4). One might have thought that the series array would have nearest-neighbor coupling, but in fact each junction is coupled equally to all the others, as (2.4) shows. (Actually, there are interactions that contribute spatially localized coupling, but they are negligibly small in the lump circuit limit.)

To non-dimensionalize the system, let

$$\omega_c = 2erI_c/\hbar, \quad t^* = \omega_c t, \quad Q^* = \omega_c Q/I_c, \quad I_b^* = I_b/I_c,$$

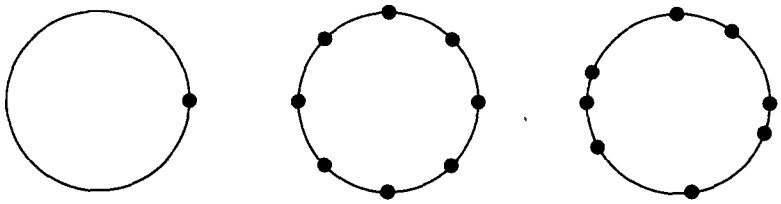

(a) in-phase state (b) splay state (c) incoherent state

Fig. 2. A rough sketch of periodic solutions of Josephson junction series arrays. Each dot on the unit circle represents the phase of a junction. (a) In-phase state: All junctions oscillate in synchrony. (b) Splay state: Phases of the junctions are scattered evenly. (c) Generic incoherent state: Phases are scattered nonuniformly.

$$L^* = \frac{\omega_c L}{rN}, \quad R^* = \frac{R}{rN}, \quad C^* = N\omega_c rC.$$

After substituting these expressions into the governing equations and dropping the asterisks, we obtain

$$\dot{\phi}_j + \sin\phi_j + \dot{Q} = I_b, \quad j = 1,\ldots,N, \tag{2.5}$$

$$L\ddot{Q} + R\dot{Q} + C^{-1}Q = \frac{1}{N}\sum_{k=1}^{N}\dot{\phi}_k, \tag{2.6}$$

where the overdot denotes differentiation with respect to dimensionless time.

Of course, there are more general loads than that shown in Fig. 1, but we will concentrate on this case since it has been studied most often in the literature. The methods to be developed in Section 3 are applicable to a broader class of loads (essentially any load describable by an integro-differential relation between current and voltage), but we will not pursue such generalities here.

2.3. *Periodic solutions of series arrays*

The system (2.5) and (2.6) involves several parameters, and its behavior can be complex. However, for both technological and mathematical reasons, the periodic solutions are the most important. They fall into three categories: in-phase, splay, and incoherent solutions.

2.3.1. *In-phase state*

As long as I_b is not too small, there is a periodic running solution of the form

$$\phi_1(t) = \phi_2(t) = \cdots = \phi_N(t) \quad \text{for all } t,$$

with a consistent $Q(t)$. If we associate each phase ϕ_j with a particle moving on the unit circle, then this *in-phase state* appears as all N particles moving together around the circle (Fig. 2a). The motion is typically non-uniform, as the analog of a whirling pendulum would suggest.

The in-phase solution is of special interest for device applications [15,16,20], because a coherently oscillating array generates much greater power than a single junction. The mathematical existence of the in-phase state is usually obvious from inspection of the governing equations. On the other hand, its stability is much more difficult to determine. A great deal of research has been devoted to this important question [15,16,18,19].

2.3.2. Splay state

A *splay state* is a periodic solution for which the individual waveforms are identical but staggered equally in time:

$$\phi_{p_1}(t) = \phi_{p_2}\left(t + \frac{1}{N}T\right) = \cdots = \phi_{p_N}\left(t + \frac{N-1}{N}T\right) \quad \text{for all } t,$$

where T is the oscillation period, and $(p_1,\ldots,p_N)$ is a permutation of $(1,\ldots,N)$. The name is motivated by the appearance of the state when plotted on a phasor diagram – the phases are "splayed" apart on the unit circle. In a sense, such a solution is maximally out of phase. In the highly special case of averaged systems, where the interactions between oscillators depend only on the *differences* of the phases [4,21], splay states are simply those in which the oscillators are evenly spaced on the circle (Fig. 2b). For further discussion of averaged systems, see Section 2.4.

It is non-trivial to prove the existence of splay states for Josephson arrays [14] or other systems of oscillators [22], although their existence is clear for averaged systems. In practice, splay states are sometimes attracting and are then found easily by numerical integration. (Further discussion of the stability of splay states is also postponed to Section 2.4.)

If a splay state exists, then in fact there are $(N-1)!$ of them, since the indices can be permuted arbitrarily without affecting the governing equations (2.5) and (2.6). This enormous multiplicity has led to the proposal that splay states could be used as possible memory states of a dynamic "multiswitch [23].

2.3.3. Continuous family of incoherent periodic solutions

A third and somewhat mysterious class of periodic solutions has been observed numerically in Josephson arrays [2,5]. These *incoherent* states are similar to splay states in that the phases are scattered on the unit circle. The difference is that the phases are not equally staggered in time.

It is an open problem to prove that such periodic solutions exist for Josephson arrays. For the trivial case of averaged systems, such solutions clearly exist; any phase configuration with its centroid at the origin will do. Note however that the higher moments need not vanish (Fig. 2c); this is what distinguishes the incoherent states from the splay state.

In averaged systems the condition of zero centroid imposes two constraints on the incoherent states; therefore they form a codimension-2 submanifold of phase space. The splay state is the most symmetric of all the incoherent states, and lies at the center of this manifold, in some sense. For more general systems, numerical evidence suggests that the incoherent states again form a low-codimension submanifold, but a proof has not been found. A possible strategy for a proof is outlined at the end of Section 4.5.

2.4. Previous results

2.4.1. Stability of the in-phase state

Early analyses of Josephson junction series arrays were based mainly on regular perturbation theory and numerical simulations [15,16]. More recent approaches have combined Floquet theory and numerics. In pioneering work, Hadley and Beasley [18] found numerically that for overdamped arrays, the in-phase state is stable if the load is inductive and unstable if it is capacitive. Hadley et al. [19] explained these results with Floquet theory, and also considered arrays with more general loads. The local stability of the in-phase state was found to depend in a complex way on the circuit

parameters. Much remains to be understood here, but we shall be concerned with a different set of questions in what follows.

2.4.2. Ubiquitous neutral stability of the splay state

Tsang et al.[7] tried to get an analytical handle on Josephson arrays by studying the simplest possible case: an array with a pure resistive load. Then $Q(t)$ can be eliminated from (2.5) and (2.6), yielding a set of N first-order equations for the phases. They showed that the system had a generalized time-reversal symmetry, which implied that the in-phase state could not be attracting. So where would trajectories go in the long run? Their numerical simulations revealed something totally unexpected: as long as I_b is not too small, all trajectories seemed to be confined to invariant 2-tori, no matter what N they considered! The tori were nested, with the splay state at the center. The invariance of the tori implied that the splay state was neutrally stable in all N directions. Tsang et al.[7] guessed that these highly non-generic results might be due to the reversibility symmetry, but that later turned out to be only part of the story.

The situation was clarified by several studies. First, Golomb et al.[5] analyzed a model system of phase oscillators, and found that the degeneracy disappeared when higher harmonics were included in the governing equations. This suggested that the pure sinusoidal form of the Josephson current relation was responsible for the original degeneracy. They also considered a model with first harmonics only:

$$\dot{\phi}_j = 1 + a\sin\phi_j + \frac{\varepsilon}{N}\sum_{k=1}^{N}\sin(\phi_k + \alpha), \quad j = 1,\ldots,N, \tag{2.7}$$

where a, ε, and α are constants. (The notation differs from their original paper.) When $\alpha = 0$, this system reduces to that studied by Tsang et al.[7]. Using linear stability analysis in the infinite-N limit, Golomb *et al.*[5] found that when $\alpha = 0$, the splay state was indeed neutrally stable in all directions. If $\alpha \neq 0$, then all but two directions were neutrally stable, regardless of the value of α.

In a complementary study, Swift et al.[4] considered the limit of weak coupling, rather than large N. They analyzed (2.7) for $\alpha = 0$ and for $|\varepsilon| \ll 1$, using the method of averaging [29,35]. This method exploits the presence of two widely separated time scales: the fast oscillations of the individual junctions occur on an $O(1)$ time scale, whereas the relative phase drift between junctions occurs on a much longer $O(1/\varepsilon)$ time scale. Swift et al. averaged over the fast oscillations to obtain a simpler *averaged system* that governs the long-term drift. The splay state of the averaged system was found to be neutrally stable in N directions, as expected. Moreover, nested 2-tori were proven to exist for the averaged system linearized about the splay state. This approach also provided accurate analytical approximations for the two frequencies on the tori.

The next round of studies revealed that splay states are neutrally stable for an unexpectedly wide class of Josephson arrays. Tsang and Schwartz [2] considered an array with a series LC-load. This system is not reversible, but they found that the splay state was still neutrally stable in an enormous number of directions: now $N-2$ Floquet multipliers were equal to $+1$. Nichols and Wiesenfeld [3] then computed the Floquet multipliers of the splay state for several kinds of loads; at least $N-2$ multipliers were always equal to $+1$. This remained true even for junctions with $\beta > 0$ (except, curiously, when the load was purely capacitive – the splay state was linearly stable in that case). Strogatz and Mirollo [6] showed that the ubiquitous neutral stability could be understood analytically in the infinite-N limit. Their approach also predicted the non-neutral

Floquet multipliers to within 0.1% of their numerically computed values.

We summarize the local stability results as follows:

Observation 1. The periodic splay state of (2.5) and (2.6) is neutrally stable in at least $N-2$ directions, for a wide range of parameters and choice of loads.

For the exceptional case of the pure resistive load, the degeneracy was observed not only locally but also globally:

Observation 2. For the resistively loaded array (2.7) with $\alpha = 0$, the splay state is neutrally stable in all N directions, for a wide range of parameters. Moreover, all trajectories seem to be confined to invariant 2-tori.

Actually, the statement about the 2-tori is now thought to be false, strictly speaking. Golomb et al.[5] and Swift [24] have shown numerically that chaotic trajectories can occur for certain choices of parameters and initial conditions. This occurs even for $N = 3$. Nonetheless, it is still intriguing that "typical" trajectories appear to lie almost exactly on 2-tori, for a fairly wide range of parameters.

2.4.3. *Hints of global structure*

The local analyses cited above do not get at the root of the degeneracy. A more global analysis is needed. Nichols and Wiesenfeld [3] expressed optimism about the possibility of progress in this direction:

> ...Under ordinary circumstances, analytic headway for nonlinear systems is notoriously difficult, without some special properties on which to capitalize. Since the neutral stability of orbits is decidedly nongeneric behavior, there must be some deep explanation for it. Moreover, since it is common to many different circuit configurations, the origin of the underlying structure must be quite general, ... This structure, in turn, may make the Josephson-junction arrays tractable, analogous to a Hamiltonian system being integrable.

We show in the following sections that this comment was prophetic.

Previously, there were indications that the key role was played by the incoherent periodic solutions (not only the splay state). In their numerical study of (2.7), Golomb et al.[5] observed that for a certain parameter range, almost all trajectories were attracted to a manifold of incoherent periodic states. Tsang and Schwartz [2] also numerically found a similar attracting manifold of periodic states in the LC-loaded Josephson arrays. Furthermore, their observations of the phase portrait of $N = 4$ oscillators led them to an important conjecture: each incoherent state has a two-dimensional surface as its basin of attraction.

These numerical results are summarized as:

Observation 3. There appears to be a manifold of incoherent periodic states. It seems to be related to the degeneracy found in the local analysis of the splay state.

In Section 4.5 we give a unified explanation of all three observations, taking care to indicate which parts of our explanation are rigorous, and which parts are plausible but still unproven.

3. Reducible systems

In this section we introduce a nonlinear transformation that explicitly reduces a fairly large class of N-dimensional oscillator systems ($N \geq 3$) to three-dimensional ones. The method is explained in Section 3.1, starting from the most general form of the equations to which the transformation applies (as far as we know). The governing equations for Josephson arrays are reducible by this transformation, as we show in Section 3.2.

3.1. Reduction

3.1.1. General reducible systems

Consider N identical phase oscillators governed by a system of ordinary differential equations of the form

$$\dot{\theta}_j = f + g\cos\theta_j + h\sin\theta_j, \qquad j = 1,\cdots,N, \tag{3.1}$$

where θ_j is the phase of the jth oscillator, and f, g, h are functions of $\theta_1, \theta_2, \cdots, \theta_N$, and 2π-periodic in each argument. (This is the simplest case. More generally, the right hand sides of (3.1) could depend explicitly on time as well as on any auxiliary dynamical variables, e.g., the charge on a load capacitor in the case of the Josephson arrays described in Section 3.2.) The key restriction is that f, g, h must not depend on the subscript j.

Intuitively, the functions f, g, h describe common *fields* determined by the states of all the oscillators. The situation is similar to that encountered in mean-field models, although the three functions are not necessarily averaged quantities of the state variables. In particular, the system need not have permutation symmetry.

3.1.2. Change of variables

The phase space for (3.1) is N-dimensional. *A priori*, a trajectory could explore the entire space. However, we are going to show that each trajectory is actually confined to a three-dimensional subspace. To see this, consider the following change of variables:

$$\tan[\tfrac{1}{2}(\theta_j(t) - \Theta(t))] = \sqrt{\frac{1+\gamma(t)}{1-\gamma(t)}}\tan[\tfrac{1}{2}(\psi_j - \Psi(t))], \quad j = 1,\cdots,N, \tag{3.2}$$

where ψ_j are *constants*, and $0 \leq \gamma < 1$. We claim that an *arbitrary* solution $\{\theta_j(t)\}$ of the system (3.1) has the form (3.2), and that it can be generated from a set of parameters $\{\psi_j\}$ that is *frozen* in time. The evolution of $\Theta(t)$, $\gamma(t)$, and $\Psi(t)$ is unknown for now. We will shortly derive the governing equations for these variables.

First, a few words about where (3.2) comes from. It was originally motivated by an analogy with the method of "variation of parameters." We had been studying a special case of (3.1) in the infinite-N limit, and we found that the transformation (3.2) arose naturally when studying the travelling waves for that system (see Section 5.3). In this simpler problem, the quantities $\Theta(t)$ and $\Psi(t)$ were simply proportional to t, and $\gamma(t)$ was constant. Later we realized that by allowing those quantities to have arbitrary time-dependence, we could apply the same transformation to the finite-N system. Another, perhaps more natural, way to motivate (3.2) has been pointed out by J. Swift (personal communication). Consider the finite-N system for the special case where f, g, h

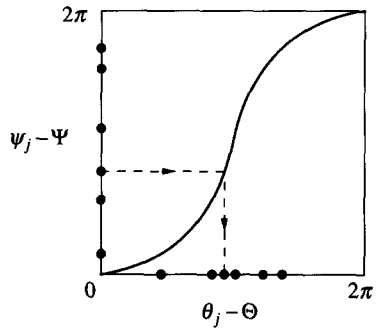

Fig. 3. Graph of the time-dependent transformation (3.2). The transformation converts solutions $\theta_j(t)$ into *constants* ψ_j. The mapping depends on a distortion parameter $\gamma(t)$, as well as two reference phases $\Theta(t)$ and $\Psi(t)$.

are constants. Then the solution for $\theta_j(t)$ can be found explicitly; it has the form of (3.2), but again with $\Theta(t)$ and $\Psi(t)$ simply proportional to t and $\gamma(t)$ constant. By variation of parameters, one is led to (3.2).

We are going to use (3.2) to change variables in (3.1), but before going into the algebra, let us consider what the transformation (3.2) means geometrically. It is a change of coordinates that relabels the phases from θ_j to ψ_j (see Fig. 3). First we go into a non-uniformly rotating coordinate system, characterized by the angle $\Theta(t)$. Then we reparametrize the circle by a time-dependent, nonlinear transformation characterized by a distortion parameter $\gamma(t)$. Finally, if we rotate again, but now according to $\Psi(t)$, we claim that *all* the oscillators appear motionless – we have converted an arbitrary solution $\{\theta_j(t)\}$ into a frozen state $\{\psi_j\}$.

The meaning of $\Theta(t)$ and $\Psi(t)$ is clear, but what does $\gamma(t)$ measure? The transformation curve of Fig. 3 is linear when $\gamma = 0$. As γ increases, the curve becomes bent and the distribution of ψ_j is increasingly distorted from that of θ_j. The curve is monotonic for all γ, so we can think of the inverse mapping in a similar manner. Now we interpret ψ_j as the preimages, and θ_j as their images. This is often the more useful point of view.

3.1.3. *Reduced equations*

Readers with a background in celestial mechanics may recognize the tranformation $\tan(v/2) = \sqrt{(1+\gamma)/(1-\gamma)}\tan(E/2)$. It appears in the analysis of the gravitational two-body problem. Here, v, E, and γ correspond to the true anomaly, the eccentric anomaly, and the eccentricity, respectively. The relation (3.2) is a time-dependent version of this transformation, with a phase shift applied to all N oscillators.

Now we rewrite (3.1) in terms of the new variables. The following formulas from classical mechanics are well known [25], and allow us to convert between our two "anomalies":

$$\sin(\theta_j - \Theta) = \frac{\sqrt{1-\gamma^2}\sin(\psi_j - \Psi)}{1 - \gamma\cos(\psi_j - \Psi)}, \quad \cos(\theta_j - \Theta) = \frac{\cos(\psi_j - \Psi) - \gamma}{1 - \gamma\cos(\psi_j - \Psi)}. \tag{3.3}$$

(To derive these formulas, one solves (3.2) for $\theta_j - \Theta$ and then applies trigonometric identities.) These formulas yield

$$\cos\theta_j = \frac{[\cos(\psi_j - \Psi) - \gamma]\cos\Theta - \sqrt{1-\gamma^2}\sin\Theta\sin(\psi_j - \Psi)}{1 - \gamma\cos(\psi_j - \Psi)},$$

$$\sin\theta_j = \frac{[\cos(\psi_j - \Psi) - \gamma]\sin\Theta + \sqrt{1-\gamma^2}\cos\Theta\sin(\psi_j - \Psi)}{1 - \gamma\cos(\psi_j - \Psi)}, \tag{3.4}$$

and these expressions are then substituted into the right hand side of (3.1).

To rewrite the left hand side of (3.1), we solve (3.2) for θ_j and differentiate with respect to time. Let $\Gamma(t) = \sqrt{(1+\gamma)/(1-\gamma)}$. Then

$$\begin{aligned}\frac{d}{dt}(\theta_j - \Theta) &= 2\frac{d}{dt}\{\arctan(\Gamma\tan[\tfrac{1}{2}(\psi_j - \Psi)])\} \\ &= \frac{2}{1 + \Gamma^2\tan^2[\frac{1}{2}(\psi_j - \Psi)]}\left(\dot\Gamma\tan[\tfrac{1}{2}(\psi_j - \Psi)] + \frac{\Gamma}{\cos^2[\frac{1}{2}(\psi_j - \Psi)]}(-\tfrac{1}{2}\dot\Psi)\right) \\ &= \frac{\Gamma}{\cos^2[\frac{1}{2}(\psi_j - \Psi)] + \Gamma^2\sin^2[\frac{1}{2}(\psi_j - \Psi)]}\left(\frac{\dot\Gamma}{\Gamma}\sin(\psi_j - \Psi) - \dot\Psi\right).\end{aligned}$$

Since

$$\begin{aligned}\cos^2[\tfrac{1}{2}(\psi_j - \Psi)] + \Gamma^2\sin^2[\tfrac{1}{2}(\psi_j - \Psi)] &= \tfrac{1}{2}(\Gamma^2 + 1) - (\Gamma^2 - 1)\cos(\psi_j - \Psi) \\ &= \frac{1 - \gamma\cos(\psi_j - \Psi)}{1 - \gamma}\end{aligned}$$

and

$$\frac{\dot\Gamma}{\Gamma} = \frac{1}{2\Gamma^2}\frac{d\Gamma^2}{dt} = \frac{1}{2\Gamma^2}\frac{d}{dt}\left(\frac{1+\gamma}{1-\gamma}\right) = \frac{\dot\gamma}{\Gamma^2(1-\gamma)^2} = \frac{\dot\gamma}{1-\gamma^2},$$

we obtain

$$\begin{aligned}\dot\theta_j &= \dot\Theta + \frac{\Gamma(1-\gamma)}{1 - \gamma\cos(\psi_j - \Psi)}\left(\frac{\dot\gamma}{1-\gamma^2}\sin(\psi_j - \Psi) - \dot\Psi\right) \\ &= \dot\Theta + \frac{\dot\gamma\sin(\psi_j - \Psi) - (1-\gamma^2)\dot\Psi}{\sqrt{1-\gamma^2}[1 - \gamma\cos(\psi_j - \Psi)]}.\end{aligned} \tag{3.5}$$

Next, substitute (3.4) and (3.5) into (3.1). After multiplying both sides by $(1 - \gamma\cos(\psi_j - \Psi))$, we obtain:

$$\begin{aligned}&\dot\Theta\,(1 - \gamma\cos(\psi_j - \Psi)) + \frac{\dot\gamma\sin(\psi_j - \Psi) - (1-\gamma^2)\dot\Psi}{\sqrt{1-\gamma^2}} = f\,(1 - \gamma\cos(\psi_j - \Psi)) \\ &+ g\{[(\cos(\psi_j - \Psi) - \gamma]\cos\Theta - \sqrt{1-\gamma^2}\sin\Theta\sin(\psi_j - \Psi)\} \\ &+ h\{[\cos(\psi_j - \Psi) - \gamma]\sin\Theta - \sqrt{1-\gamma^2}\cos\Theta\sin(\psi_j - \Psi)\}, \quad j = 1, \cdots, N.\end{aligned}$$

The terms above can be organized as a linear combination of 1, $\cos(\psi_j - \Psi)$, and $\sin(\psi_j - \Psi)$. The fact that no higher harmonics are generated is remarkable. This is the crucial property that underlies the success of the reduction procedure.

Now writing out the linear combination with the appropriate coefficients in brackets, we obtain:

$$0 = (\dot{\Theta} - \sqrt{1-\gamma^2}\dot{\Psi} - f + g\gamma\cos\Theta + h\gamma\sin\Theta)$$
$$+ \cos(\psi_j - \Psi)(-\gamma\dot{\Theta} + \gamma f - g\cos\Theta - h\sin\Theta)$$
$$+ \sin(\psi_j - \Psi)\left(\frac{\dot{\gamma}}{\sqrt{1-\gamma^2}} + g\sqrt{1-\gamma^2}\sin\Theta - h\sqrt{1-\gamma^2}\cos\Theta\right), \quad j = 1,\cdots,N.$$

Observe that the coefficients do not depend on j since we have assumed that f, g, and h do not depend on j. Thus the equations will be satisfied identically *for all j and for all t* if the three coefficients vanish independently. This can be achieved if the unknown functions γ, Θ, Ψ evolve according to

$$\dot{\gamma} = -(1-\gamma^2)(g\sin\Theta - h\cos\Theta), \quad \gamma\dot{\Psi} = -\sqrt{1-\gamma^2}(g\cos\Theta + h\sin\Theta),$$
$$\gamma\dot{\Theta} = \gamma f - g\cos\Theta - h\sin\Theta. \tag{3.6}$$

This is a closed system for (γ, Ψ, Θ) since $\theta_1, \cdots, \theta_N$ in the functions f, g, h can be expressed in terms of these new dependent variables via (3.2). The frozen phases $\{\psi_j\}$ of the N oscillators appear in the system merely as parameters. As long as these three ordinary differential equations are satisfied, $\{\theta_j(t)\}$ is guaranteed to satisfy the N equations (3.1).

3.1.4. Converting initial conditions

Given the reduced system (3.6), two questions immediately arise: how do we obtain initial conditions for the "reduced variables" (γ, Ψ, Θ) to start integrating (3.6), and how do we determine the "system constants" $\{\psi_j\}$? Given an arbitrary initial condition $\{\theta_j(0)\}$ in the old coordinates, we need to convert these N values to the new set of $N+3$ values $\{\psi_j\}, \gamma(0), \Psi(0), \Theta(0)$ so that (3.2) is satisfied at $t = 0$. The equations (3.2) provide N constraints, but we have $N + 3$ unknowns. Hence there are many ways to achieve this conversion.

One natural choice is to evolve from the "identity conversion":

$$\gamma(0) = \Theta(0) = \Psi(0) = 0, \quad \psi_j = \theta_j(0), \qquad j = 1,\ldots,N, \tag{3.7}$$

by which (3.2) is trivially satisfied at $t = 0$. In Section 4.2 we shall see that another way of converting initial conditions provides much more insight into the phase space structure. For the moment, however, we are content to observe that there is at least one way to reduce the N-dimensional problem to a three-dimensional one. Since (3.7) shows that an arbitrary initial condition can be converted, we conclude that (3.2) expresses the *general* solution of the system (3.1).

3.1.5. Removing a coordinate singularity

Another question regarding (3.6) is that the equations, in general, cease to be valid at $\gamma = 0$. Unless g, $h \to 0$ as $\gamma \to 0$, $\dot{\Theta}$ and $\dot{\Psi}$ become singular. At the same time, $\dot{\gamma} < 0$ seems possible at $\gamma = 0$ so that γ might not stay positive, contrary to its definition. Such troubles are only artifacts of a coordinate singularity, and can be avoided in the following manner.

The system (3.6) involves one amplitude variable γ and two phase variables Θ and Ψ. To avoid the singularity at $\gamma = 0$, we introduce a Cartesian-type coordinate system

$$x = \gamma\cos\Theta, \quad y = \gamma\sin\Theta, \quad \Phi = \Theta - \Psi, \quad (x^2 + y^2 < 1). \tag{3.8}$$

Then

$$\begin{aligned}\dot{x} &= \dot{\gamma}\cos\Theta - \gamma\dot{\Theta}\sin\Theta \\ &= -(1-\gamma^2)(g\sin\Theta - h\cos\Theta)\cos\Theta - \sin\Theta(\gamma f - g\cos\Theta - h\sin\Theta) \\ &= -\gamma f\sin\Theta + \gamma^2 g\sin\Theta\cos\Theta + h(1-\gamma^2\cos^2\Theta) \\ &= -yf + xyg + (1-x^2)h. \end{aligned} \tag{3.9}$$

Similarly,

$$\dot{y} = xf - (1-y^2)g - xyh. \tag{3.10}$$

The angle Φ is defined in such a way to subtract out singularities of the two phase equations. Thus,

$$\begin{aligned}\gamma^2\dot{\Phi} &= \gamma^2\dot{\Theta} - \gamma^2\dot{\Psi} \\ &= \gamma(\gamma f - g\cos\Theta - h\sin\Theta) + \gamma\sqrt{1-\gamma^2}(g\cos\Theta + h\sin\Theta) \\ &= \gamma^2 f - (1-\sqrt{1-\gamma^2})(\gamma g\cos\Theta + \gamma h\sin\Theta) \\ &= \gamma^2 f - (1-\sqrt{1-\gamma^2})(xg + yh).\end{aligned}$$

Hence,

$$\dot{\Phi} = f - \frac{1-\sqrt{1-\gamma^2}}{\gamma^2}(xg + yh). \tag{3.11}$$

At $\gamma = 0$, Eqs. (3.9)–(3.11) reduce to a well-behaved set of equations:

$$\dot{x} = h, \quad \dot{y} = -g, \quad \dot{\Phi} = f. \tag{3.12}$$

The initial conditions and the system constants are obtained in this coordinate system by rewriting (3.7):

$$x(0) = y(0) = \Phi(0) = 0, \qquad \psi_j = \theta_j(0), \quad j = 1,\ldots,N. \tag{3.13}$$

When a trajectory passes through the origin $\gamma = 0$ in (3.6), Θ and Ψ jump discontinuously by $\pm\pi$. In this new coordinate system, however, their difference Φ still changes continuously. Since γ is now computed by $\gamma = \sqrt{x^2+y^2}$, it remains non-negative. When $\gamma = 0$, Θ and Ψ are not determined. This is reasonable, and poses no problems because we can still compute θ_j via (3.2). For $\gamma = 0$, we find

$$\theta_j = \Theta + (\psi_j - \Psi) = \psi_j + \Phi.$$

So, we do not need to know Θ and Ψ but only their difference Φ. The coordinate singularity at $\gamma = 0$ is resolved in this way.

3.2. Josephson junction arrays as reducible systems

3.2.1. Reduction

The reduction method of the previous section is immediately applicable to the Josephson junction array equations (2.5) and (2.6). To see this, we note that the N equations (2.5) have the form of (3.1) where $\theta_j = \phi_j$, $f = I_B - \dot{Q}$, $g = 0$, and $h = -1$. The function f depends on another dynamical variable $\dot{Q}$, but there is no difference in the reduction procedure. Since we derived the

reduced equations (3.9)–(3.11) from (3.1) without applying any operations on f, g, and h, the reduction is still valid even when these functions depend on auxiliary dynamical variables or on time explicitly. The N phase equations can be satisfied by integrating only three equations, but now they are coupled with the evolution equations for the non-reducible auxiliary variables. Specifically, the equations (2.5) and (2.6) become

$$\begin{aligned} \dot{x} &= -y(I_B - \dot{Q}) - (1 - x^2) && \text{from (3.9)}, \\ \dot{y} &= x(I_B - \dot{Q}) + xy && \text{from (3.10)}, \\ \dot{\Phi} &= (I_B - \dot{Q}) + \frac{1 - \sqrt{1 - \gamma^2}}{\gamma^2} y && \text{from (3.11)}, \end{aligned} \tag{3.14}$$

with

$$L\ddot{Q} + R\dot{Q} + C^{-1}Q = \frac{1}{N}\sum_{k=1}^{N}(I_B - \dot{Q} - \sin\phi_k)\,. \tag{3.15}$$

ϕ_k is expressed by x, y, Φ through the transformation.

It is clear that (3.14) and (3.15) is equivalent to a fifth-order system of ordinary differential equations with variables $(x, y, \Phi, Q, \dot{Q})$ when $L \neq 0$. When $L = 0$, (3.15) can be solved for $\dot{Q}$ to obtain a fourth-order system with variables (x, y, Φ, Q). In any case, we have reduced the N equations (2.5) to three equations (3.14).

3.2.2. Relation to neutral stability

Any trajectory of these Josephson junction arrays is, therefore, confined to a subspace of $N - 3$ fewer dimensions than the whole phase space. Three dimensions of the subspace are accounted for by the transformation (3.2); by allowing γ, Ψ, Θ to vary for fixed $\{\psi_j\}$, the image $\{\theta_j\}$ sweeps out a three-dimensional manifold. Choosing a different set of $\{\psi_j\}$ would produce another manifold. The product of such a manifold with the auxiliary directions (Q and $\dot{Q}$ if necessary) is the subspace from which a trajectory cannot escape.

These facts are reminiscent of Observation 1 in Section 2.4, which deals with the widespread occurrence of $N - 2$ neutral directions. If one computes the Floquet multipliers of a periodic orbit, one of them is always $+1$, corresponding to perturbations along the orbit. The other $N - 3$ unit multipliers must correspond to the number of dimensions we have reduced. The precise connection will not become clear until Section 4.5, when we demonstrate the foliation of phase space by invariant subspaces. This foliation is the source of the ubiquitous neutral stability.

3.2.3. Chaotic dynamics in resistively loaded arrays

What behavior do we expect from the reduced systems? Although this question has not yet been investigated in general, there is preliminary evidence of complicated behavior.

Consider a purely resistively loaded array. The governing equations are then given by (2.7) with $\alpha = 0$:

$$\dot{\phi}_j = 1 + a\sin\phi_j + \frac{\varepsilon}{N}\sum_{k=1}^{N}\sin\phi_k\,, \quad j = 1, \cdots, N\,. \tag{3.16}$$

Assume that $|a + \varepsilon| < 1$, so that there are no fixed points [5,7]. Then trajectories typically appear to lie on 2-tori as in Observation 2 of Section 2.4. However, Golomb et al.[5,26] found numerical

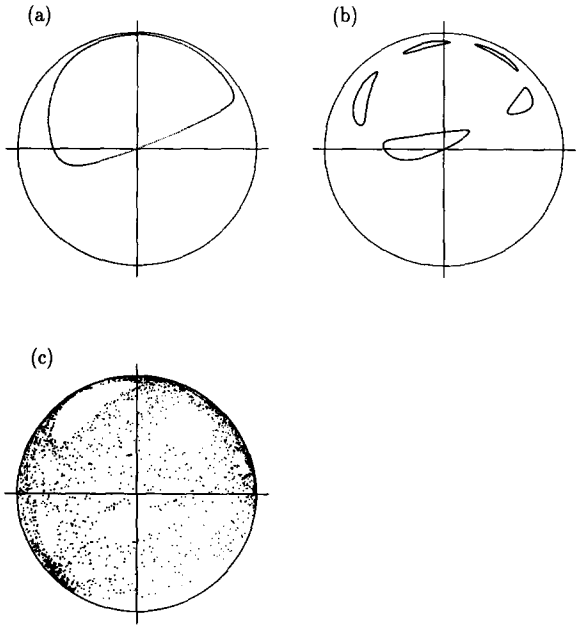

Fig. 4. Poincaré sections of the reduced system (3.17) at $\Phi = 0 \pmod{2\pi}$ for $N = 3$ junctions. Each section shows one trajectory starting at $x = y = \Phi = 0$ at $t = 0$. The initial conditions are $\phi_1(0) = 3\pi/5$, $\phi_2(0) = 0$, $\phi_3(0) = -7\pi/10$. The identity conversion (3.13) requires the preimages to be $\psi_j = \phi_j(0)$. These values are fixed in time.
(a) $a = 1$, $\varepsilon = -0.7$. The section shows an invariant closed curve, suggesting that the trajectory lies on a 2-torus in the original phase space. (b) $a = 1$, $\varepsilon = -1.95$. Period-5 islands. (c) $a = 1.5$, $\varepsilon = -0.7$. Chaos.

evidence for aperiodic trajectories for systems as small as $N = 6$, depending on the parameters a and ε. Swift [24] further demonstrated numerically that chaos occurs even for $N = 3$. He transformed the three angles ϕ_j linearly into the mean phase $\bar{\phi}$ and two phase differences. Since $\bar{\phi}$ is monotonically increasing when $|a + \varepsilon| < 1$, the Poincaré return map at $\bar{\phi} = 0 \pmod{2\pi}$ is well defined. Depending on the parameters, chaotic-looking Poincaré sections were obtained.

We employ the same idea, but using the nonlinear reduction. The equations (3.16) reduce to the three equations corresponding to the special case of (3.14) and (3.15):

$$\dot{x} = -y\left(1 + \frac{\varepsilon}{N}\sum_{k=1}^{N}\sin\phi_k\right) + a(1-x^2), \quad \dot{y} = x\left(1 + \frac{\varepsilon}{N}\sum_{k=1}^{N}\sin\phi_k\right) - axy,$$

$$\dot{\Phi} = 1 + \frac{\varepsilon}{N}\sum_{k=1}^{N}\sin\phi_k - ay\frac{1-\sqrt{1-y^2}}{y^2}, \tag{3.17}$$

where $\phi_k = \phi_k(x, y, \Phi; \{\psi_j\})$ is given by the transformation (3.2), and $y = \sqrt{x^2 + y^2}$. Here Φ plays a similar role to the mean phase of the ϕ's.

Now (3.17) is numerically integrated, and every time $\Phi = 0 \pmod{2\pi}$, a point (x, y) is plotted. (The initial condition is converted by (3.13).) Fig. 4 shows three Poincaré sections obtained for $N = 3$ using a randomly chosen set of $\phi_1(0)$, $\phi_2(0)$, and $\phi_3(0)$.

Fig. 4a shows the section when $a = 1, \varepsilon = -0.7$. We find a set of points on a closed curve; the trajectory is (very nearly) on a 2-torus, and is quasiperiodic. The closed curve passes through the origin because the conversion (3.13) requires the trajectory to start from $x = y = \Phi = 0$ at $t = 0$.

Fig. 4b shows the case $a = 1, \varepsilon = -1.95$. The section produced by *one* trajectory looks like islands surrounding a period-5 orbit.

Fig. 4c is the case $a = 1.5, \varepsilon = -0.7$. This section is clearly chaotic.

These results suggest that the system has invariant tori that break as parameters are varied, a behavior familiar from weakly non-integrable systems [27–29], such as the Hénon-Heiles system [30]. However, the flow here is not Hamiltonian nor even volume-preserving, although it is reversible. The Poincaré map appears to be area-preserving, but only if Φ is strobed at multiples of 2π. Perhaps the KAM theory for reversible flows [31] can be used to shed light on the numerical observations above.

4. Global structure

To make further analytical progress, we consider the limit of weakly coupled arrays. Averaging theory leads to a simpler set of equations that can be analyzed completely.

The equations considered in this section are a generalization of those studied by Swift et al. [4]. They averaged the resistive load equations (3.16), assuming that $|a| < 1$ and $|\varepsilon| \ll 1 - |a|$. The averaged equations were found to take the form

$$\dot{\theta}_j = \omega + \frac{1}{N}\sum_{k=1}^{N} \cos(\theta_k - \theta_j), \quad j = 1, \ldots, N,$$

where ω is a constant, and time has been rescaled. The variable θ_j is a nonlinearly transformed version of the phase ϕ_j in (3.16).

Swift [32] later derived the more general averaged equations governing (2.5) and (2.6) with an arbitrary *RLC* load. Weak coupling was put in by hand, by inserting a small parameter in front of $\dot{Q}$ in (2.5). The resulting equations [32] are

$$\dot{\theta}_j = \omega + \frac{1}{N}\sum_{k=1}^{N} \cos(\theta_k - \theta_j - \delta), \quad j = 1, \ldots, N \tag{4.1}$$

where δ is a parameter that depends on the values of R, L, C, and I_b.

The averaged equations (4.1) are of interest beyond their connection to Josephson arrays. For instance, when averaging theory is applied to the system (2.7) of Golomb et al. in the limit of weak coupling, one again obtains (4.1). In this case δ is given by $\sin\delta = (\text{sign}\varepsilon)\sin\alpha$. Eq. (4.1) also appears as the averaged system for globally coupled van der Pol oscillators with linear coupling [33], and for a globally coupled version of the complex Ginzburg-Landau equation [34]. Finally, from a mathematical point of view, (4.1) is perhaps the simplest nontrivial N-body system coupled by nonlinear interactions.

In Section 4.1, we derive and analyze the reduced equations for (4.1). Section 4.2 presents a way of converting initial conditions that is much more illuminating than the identity conversion (3.7). This new conversion is used in Section 4.3 to provide global information about the dynamics of (4.1). Section 4.4 presents numerical illustrations of the results.

We will see that the phase space of (4.1) possesses highly degenerate global structures. Some of them persist in the Josephson array equations (2.5) and (2.6) *before* averaging. Section 4.5

discusses which structures survive, and explains the three observations previously made in Section 2.4.

4.1. Reduction of averaged systems

In a frame rotating at angular velocity ω, (4.1) is equivalent to

$$\dot{\theta}_j = \frac{1}{N}\sum_{k=1}^{N}\cos(\theta_k - \theta_j - \delta), \quad j = 1,\ldots,N. \tag{4.2}$$

Thus the constant ω does not affect the essential dynamics. Eq. (4.2) is in the form of (3.1), where

$$f = 0, \quad g = \frac{1}{N}\sum_{k=1}^{N}\cos(\theta_k - \delta), \quad h = \frac{1}{N}\sum_{k=1}^{N}\sin(\theta_k - \delta). \tag{4.3}$$

The reduced equations in the polar expression (3.6) become

$$\dot{\gamma} = \frac{1-\gamma^2}{N}\sum_{k=1}^{N}\sin(\theta_k - \Theta - \delta), \quad \gamma\dot{\Psi} = -\frac{\sqrt{1-\gamma^2}}{N}\sum_{k=1}^{N}\cos(\theta_k - \Theta - \delta),$$

$$\gamma\dot{\Theta} = -\frac{1}{N}\sum_{k=1}^{N}\cos(\theta_k - \Theta - \delta).$$

We intentionally use these polar coordinates instead of their Cartesian counterpart. Although a coordinate singularity arises, it causes no trouble, as will be seen in Section 4.2.

Using the formula (3.3), this set of equations becomes

$$\begin{aligned}
\dot{\gamma} &= \cos\delta\frac{(1-\gamma^2)^{3/2}}{N}\sum_{k=1}^{N}\frac{\sin(\psi_k - \Psi)}{1-\gamma\cos(\psi_k - \Psi)} + \sin\delta\frac{1-\gamma^2}{N}\sum_{k=1}^{N}\frac{\gamma - \cos(\psi_k - \Psi)}{1-\gamma\cos(\psi_k - \Psi)},\\
\gamma\dot{\Psi} &= \cos\delta\frac{(1-\gamma^2)^{1/2}}{N}\sum_{k=1}^{N}\frac{\gamma - \cos(\psi_k - \Psi)}{1-\gamma\cos(\psi_k - \Psi)} - \sin\delta\frac{1-\gamma^2}{N}\sum_{k=1}^{N}\frac{\sin(\psi_k - \Psi)}{1-\gamma\cos(\psi_k - \Psi)},\\
\gamma\dot{\Theta} &= \cos\delta\frac{1}{N}\sum_{k=1}^{N}\frac{\gamma - \cos(\psi_k - \Psi)}{1-\gamma\cos(\psi_k - \Psi)} - \sin\delta\frac{(1-\gamma^2)^{1/2}}{N}\sum_{k=1}^{N}\frac{\sin(\psi_k - \Psi)}{1-\gamma\cos(\psi_k - \Psi)}.
\end{aligned} \tag{4.4}$$

The system looks intimidating, but it is actually very simple. First, notice that Θ has disappeared from the right hand sides. Hence the dynamics is determined only by (Ψ,γ) while Θ is driven passively by them. Since the dynamics is effectively *two*-dimensional, we know immediately that the system is never chaotic.

Second, note that there are only two types of sums on the right hand sides of (4.4). The form of these sums suggests that they might be partial derivatives of a common function. Indeed, a useful function can be constructed as follows. If we define

$$\mathcal{H}(\Psi,\gamma) = \frac{1}{N}\sum_{k=1}^{N}\log\left(\frac{1-\gamma\cos(\psi_k - \Psi)}{\sqrt{1-\gamma^2}}\right), \tag{4.5}$$

then we produce the two sums mentioned just above:

$$\frac{\partial \mathcal{H}}{\partial \Psi} = -\frac{1}{N}\sum_{k=1}^{N} \frac{\gamma \sin(\psi_k - \Psi)}{1 - \gamma\cos(\psi_k - \Psi)} \tag{4.6}$$

and

$$\begin{aligned}\frac{\partial \mathcal{H}}{\partial \gamma} &= \frac{\partial}{\partial \gamma}\left(-\tfrac{1}{2}\log(1-\gamma^2) + \frac{1}{N}\sum_{k=1}^{N}\log[1-\gamma\cos(\psi_k - \Psi)]\right) \\ &= \frac{\gamma}{1-\gamma^2} - \frac{1}{N}\sum_{k=1}^{N}\frac{\cos(\psi_k - \Psi)}{1-\gamma\cos(\psi_k - \Psi)} \\ &= \frac{1}{N(1-\gamma^2)}\sum_{k=1}^{N}\frac{\gamma - \cos(\psi_k - \Psi)}{1-\gamma\cos(\psi_k - \Psi)}\,. \end{aligned} \tag{4.7}$$

Thus we can express the (γ, Ψ)-dynamics of (4.4) as:

$$\begin{aligned}\frac{\dot{\gamma}}{1-\gamma^2} &= -\frac{\sqrt{1-\gamma^2}}{\gamma}\frac{\partial \mathcal{H}}{\partial \Psi}\cos\delta + (1-\gamma^2)\frac{\partial \mathcal{H}}{\partial \gamma}\sin\delta\,, \\ \frac{\dot{\Psi}}{1-\gamma^2} &= +\frac{\sqrt{1-\gamma^2}}{\gamma}\frac{\partial \mathcal{H}}{\partial \gamma}\cos\delta + \frac{1}{\gamma^2}\frac{\partial \mathcal{H}}{\partial \Psi}\sin\delta\,. \end{aligned} \tag{4.8}$$

4.1.1. Hamiltonian when $\sin\delta = 0$

When $\sin\delta = 0$, the system becomes completely integrable. Consider, for example, the case $\delta = 0$. (The case $\delta = \pi$ is similar.) Then (4.8) shows that $\mathcal{H}$ is conserved:

$$\dot{\mathcal{H}} = \dot{\gamma}\frac{\partial \mathcal{H}}{\partial \gamma} + \dot{\Psi}\frac{\partial \mathcal{H}}{\partial \Psi} = (1-\gamma^2)\left[\left(-\frac{\sqrt{1-\gamma^2}}{\gamma}\frac{\partial \mathcal{H}}{\partial \Psi}\right)\frac{\partial \mathcal{H}}{\partial \gamma} + \left(\frac{\sqrt{1-\gamma^2}}{\gamma}\frac{\partial \mathcal{H}}{\partial \gamma}\right)\frac{\partial \mathcal{H}}{\partial \Psi}\right] = 0\,.$$

For this case, we could express (4.8) as a *one degree-of-freedom* Hamiltonian system. To see this, let $\alpha = 1/\sqrt{1-\gamma^2}$. Then (4.8) becomes

$$\dot{\alpha} = -\frac{\partial \mathcal{H}}{\partial \Psi}\,, \quad \dot{\Psi} = +\frac{\partial \mathcal{H}}{\partial \alpha}$$

which is in Hamiltonian form. The appropriate phase space for this system is a cylinder, since $\mathcal{H}$ is periodic in Ψ. The trajectories lie on contours of $\mathcal{H}$, and are typically closed orbits (or fixed points in exceptional cases). Hence $\Psi(t), \alpha(t)$, and therefore $\gamma(t)$ are typically periodic in t.

What can we say about the remaining Θ-direction? In (4.4), Θ does not appear on the right hand sides. In particular, $\dot{\Theta}$ is dependent only on (Ψ, γ). Suppose after one period T of the (Ψ, γ) motion, Θ shifts by some amount, say $\Theta(t+T) = \Theta(t) + 2\pi W$, where W denotes the winding number. Then, since Ψ and γ have returned to their starting values, the same shift of Θ occurs on all following cycles. Therefore, when $\sin\delta = 0$, the solutions of (4.4) are typically quasiperiodic, with trajectories confined to invariant 2-tori. Thus (4.1) is completely integrable when $\sin\delta = 0$.

4.1.2. Lyapunov function for general δ

When $\sin\delta \neq 0$, we may still compute $\dot{\mathcal{H}}$ from (4.8). As before, terms involving $\cos\delta$ vanish, and now we obtain:

$$\dot{\mathcal{H}} = P \sin\delta, \tag{4.9}$$

where

$$P(\Psi, \gamma, \{\psi_j\}) = (1-\gamma^2)\left[(1-\gamma^2)\left(\frac{\partial \mathcal{H}}{\partial \gamma}\right)^2 + \frac{1}{\gamma^2}\left(\frac{\partial \mathcal{H}}{\partial \Psi}\right)^2\right]$$

is a positive definite function since $0 < \gamma < 1$. (Again, there is slight ambiguity at $\gamma = 0$.) Thus, $\mathcal{H}$ acts as a Lyapunov function in this general case, and the sign of $\sin\delta$ determines the direction of change in $\mathcal{H}$.

To interpret the function P more intuitively, substitute (4.6) and (4.7) back into the right hand side of (4.9):

$$P = \left(\frac{1}{N}\sum_{k=1}^{N} \frac{\gamma - \cos(\psi_k - \Psi)}{1 - \gamma\cos(\psi_k - \Psi)}\right)^2 + \left(\frac{1}{N}\sum_{k=1}^{N} \frac{\sqrt{1-\gamma^2}\sin(\psi_k - \Psi)}{1 - \gamma\cos(\psi_k - \Psi)}\right)^2.$$

Using the formula (3.3) also in reverse,

$$P = \left(\frac{1}{N}\sum_{k=1}^{N} \cos(\theta_k - \Theta)\right)^2 + \left(\frac{1}{N}\sum_{k=1}^{N} \sin(\theta_k - \Theta)\right)^2.$$

Define

$$R(t)\exp[i\phi(t)] = \frac{1}{N}\sum_{k=1}^{N} \exp(i\theta_k), \quad R \geq 0,\ \phi \in \mathbb{R}, \tag{4.10}$$

which denotes the "order parameter", or the centroid vector of the N oscillators located on a unit circle according to their phase angles. Then

$$P = [R\cos(\phi - \Theta)]^2 + [R\sin(\phi - \Theta)]^2 = R^2.$$

Hence $\dot{\mathcal{H}} = R^2 \sin\delta$. So $\mathcal{H}$ is stationary only when $R = 0$, i.e., when the N oscillators are distributed such that their centroid vanishes. From (4.10), these special states satisfy

$$\frac{1}{N}\sum_{k=1}^{N} \cos\theta_k = \frac{1}{N}\sum_{k=1}^{N} \sin\theta_k = 0. \tag{4.11}$$

States satisfying (4.11) play an important role in the rest of the article. From now on, we refer to them as "incoherent" states of the averaged systems.

4.1.3. Remaining issues

Two issues still need to be addressed:

(1) The analysis could potentially fail when $\gamma = 0$. As discussed in Section 3.1, the reduced equations (4.4) can become singular at this value.
(2) We would like to visualize the Lyapunov function $\mathcal{H}$. For instance, what do its level curves look like? And what is the meaning of increasing or decreasing $\mathcal{H}$?

These matters are resolved in the next two sections by locating the incoherent states at the center of a picture that clarifies everything.

4.2. Constraints and constants of motion

4.2.1. Choice of constraints

In this section we reconsider how to convert the original initial conditions $\{\theta_j(0)\}$ into the initial conditions of the reduced variables $\{\gamma(0), \Theta(0), \Psi(0)\}$ and the system constants $\{\psi_j\}$. As explained in Section 3.1, there are many ways to achieve this conversion. Since we determine $N + 3$ values from N constraints, three additional constraints may be imposed to eliminate the multiplicity of the conversion. In Section 3.1 we showed one way of achieving this, namely the identity transformation (3.7). In this approach, *all three constraints are imposed on the reduced variables*, that is, we required that $\gamma(0) = \Psi(0) = \Theta(0) = 0$.

Although it shows that the reduction is valid, this approach is not suitable if one wants to take a global view of the system. Here is the drawback: using (3.7), each initial condition $\{\theta_j(0)\}$ yields different system constants $\{\psi_j\}$ so that the flow (3.6) itself is changed whenever the initial condition is replaced. All solutions originate from the same point $\gamma = \Theta = \Psi = 0$, and evolve under different flows (3.6). Both of these features are confusing and ungeometric: normally we want different solutions to start from *different* points in phase space, and to evolve under the *same* flow.

A better choice of the constraints is to impose all three of them on the system constants rather than on the reduced variables. In this way, we are able to vary initial conditions of the reduced variables while keeping the system constants the same. By changing initial conditions $\gamma(0)$, $\Psi(0)$, and $\Theta(0)$ over their full ranges, a three-dimensional family of trajectories is bundled together and distinguished from all others by the marker $\{\psi_j\}$. The parameters $\{\psi_j\}$ specify a three-dimensional invariant subspace in the original phase space, and therefore can be interpreted as a set of constants of motion. Since there are three constraints on them, the number of *independent* constants of motion is $N - 3$. The whole phase space of $\{\theta_j\}$ is, in this way, decomposed into an $(N - 3)$-parameter family of invariant subspaces.

4.2.2. Parametrization by incoherent states

What are the appropriate constraints to impose on the $\{\psi_j\}$? One of them turns out to be somewhat arbitrary, as we'll see below, while the remaining two constraints are quite natural – they are suggested by the form of the averaged equations (4.4) at $\gamma = 0$.

For $\gamma = 0$, the polar coordinate expression of the reduced equations becomes singular (as expected from Section 3.1). However, this singularity poses no problem (even without resorting to Cartesian expressions) by choosing appropriate constraints on $\{\psi_j\}$. When $\gamma = 0$, the first equation of (4.4) becomes

$$\dot{\gamma} = \frac{1}{N}\sum_{k=1}^{N}[\cos\delta\sin(\psi_k - \Psi) - \sin\delta\cos(\psi_k - \Psi)] = \frac{1}{N}\sum_{k=1}^{N}\sin(\psi_k - \Psi - \delta).$$

We impose two constraints:

$$\frac{1}{N}\sum_{k=1}^{N}\cos\psi_k = \frac{1}{N}\sum_{k=1}^{N}\sin\psi_k = 0. \tag{4.12}$$

Then

$$\dot{\gamma} = \frac{\cos(\Psi + \delta)}{N} \sum_{k=1}^{N} \sin \psi_k - \frac{\sin(\Psi + \delta)}{N} \sum_{k=1}^{N} \cos \psi_k = 0$$

so that $\gamma = 0$ becomes *stationary*. When $\gamma = 0$, the transformation (3.2) reduces to

$$\theta_j(t) = \psi_j + [\Theta(t) - \Psi(t)] .$$

Hence, regardless of $(\Theta - \Psi)$, we find

$$\frac{1}{N} \sum_{k=1}^{N} \cos \theta_k = \frac{1}{N} \sum_{k=1}^{N} \sin \theta_k = 0 \quad \text{for all } t, \tag{4.13}$$

and, from (4.2),

$$\dot{\theta}_j = 0 \quad \text{for all } j \text{ and } t.$$

The condition (4.13) is the same as (4.11), i.e., the phases are "incoherent". These states are fixed points of the system (4.2), or rigidly rotating periodic solutions of (4.1) in the original frame. The condition $\gamma = 0$ is now synonomous with the subspace of incoherent states, thanks to (4.12). This subspace is *invariant* under the flow.

The second and third equations of (4.4) are also satisfied consistently by imposing (4.12). Their right hand sides clearly vanish when $\gamma = 0$, as does the coefficient γ of the left hand sides. Now, $\dot{\Psi}$ and $\dot{\Theta}$ do not have to diverge. In fact, Ψ and Θ can be arbitrary as long as $\dot{\Psi} = \dot{\Theta}$ (required from $\gamma \to 0$ limit of (4.4)). This is consistent with the fact that the mapping curve (3.2) is linear when $\gamma = 0$, therefore, we do not need the values of Ψ and Θ themselves.

By imposing the natural constraints (4.12), we have made the polar coordinate expression (4.4) valid everywhere. The constraints are imposed on the system constants, and therefore have a more natural geometric interpretation.

4.2.3. Convertibility of initial conditions

When the new constraints (4.12) are imposed, a new problem arises: given an arbitrary initial condition $\{\theta_j(0)\}$ of the original system, we need to be able to convert it into reduced variables $\gamma(0)$, $\Theta(0)$, $\Psi(0)$ and system constants $\{\psi_j\}$, subject to the constraint that the $\{\psi_j\}$ be incoherent. Is such a conversion possible for an arbitrary initial condition $\{\theta_j(0)\}$? If not, then (3.2) would represent only a particular solution, rather than the general solution of the system. The following lemma shows that such a conversion is indeed possible for almost all initial conditions.

Lemma. For almost all values of $\theta_1, \cdots, \theta_N$, there exist reduced variables γ, Θ, Ψ, and constants $\psi_1, \cdots, \psi_N$ such that (3.2) and (4.12) are both satisfied. The only exceptions are "majority clusters" in which $N/2$ or more of the θ_j are equal (mod 2π).

Remark. The following proof will show why majority clusters are special.

Proof. Since (3.2) is invariant under

$$\theta_j \leftrightarrow \psi_j, \quad \Theta \leftrightarrow \Psi, \quad \gamma \to (-\gamma), \tag{4.14}$$

the formulas (3.3) and (3.4) are, too. Therefore the two equations in (3.3) become

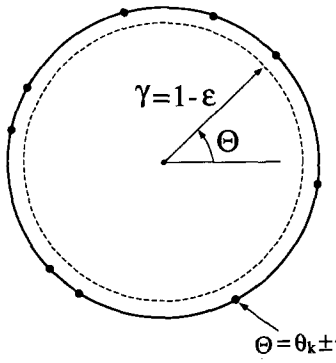

Fig. 5. Index theory is applied to the region inside the dashed circle of radius $1-\epsilon$, $\epsilon \to 0+$. The radial and angular coordinates are γ and Θ, respectively. For each phase θ_k, $\Theta = \theta_k \pm \pi$ on the unit circle becomes a singular point of the vector field (V_γ, V_Θ).

$$\sin(\psi_j - \Psi) = \frac{\sqrt{1-\gamma^2}\sin(\theta_j - \Theta)}{1+\gamma\cos(\theta_j - \Theta)}, \quad \cos(\psi_j - \Psi) = \frac{\gamma + \cos(\theta_j - \Theta)}{1+\gamma\cos(\theta_j - \Theta)}. \tag{4.15}$$

Thus, (4.12) is equivalent to:

$$V_\Theta \triangleq \frac{1}{N}\sum_{k=1}^{N} \frac{\gamma\sin(\theta_k - \Theta)}{1+\gamma\cos(\theta_k - \Theta)} = 0, \quad V_\gamma \triangleq \frac{1}{N}\sum_{k=1}^{N} \frac{\gamma + \cos(\theta_k - \Theta)}{1+\gamma\cos(\theta_k - \Theta)} = 0. \tag{4.16}$$

Here, the θ_k are given and fixed, and we seek a solution (Θ, γ) in the allowed region $0 \le \Theta < 2\pi$, $0 \le \gamma < 1$. The strategy is to interpret a solution (Θ, γ) as a fixed point of a continuous vector field defined by (V_Θ, V_γ), and then to use index theory to prove that the vector field has a fixed point.

If we interpret Θ and γ as the angle and radius in polar coordinates (Fig. 5), then the allowed region corresponds to the unit disk, and V_Θ and V_γ represent the angular and radial components of a vector field, respectively. The vector field is continuous in the open disk $0 \le \gamma < 1$. On the circle $\gamma = 1$, (4.16) shows that V_Θ diverges at $\Theta = \theta_k \pm \pi$ for $k = 1, \ldots, N$. Thus, when computing the index, we choose a slightly smaller circle $\gamma = 1 - \epsilon$, and then take $\epsilon \to 0+$.

How does V_γ change on this circle? The denominator of the kth term of V_γ, i.e., $(1+\gamma\cos(\theta_k - \Theta))$, vanishes at $\gamma = 1$ and $\theta_k - \Theta = \pm\pi$. However, the numerator $(\gamma + \cos(\theta_k - \Theta))$ also vanishes. To resolve the kth term around this singularity, let $\gamma = 1-\epsilon$ and $\mu = \Theta - \theta_k \pm \pi$ where $0 < \epsilon, |\mu| \ll 1$. Then

$$\frac{1}{N}\frac{\gamma + \cos(\theta_k - \Theta)}{1+\gamma\cos(\theta_k - \Theta)} = \frac{1}{N}\frac{1-\epsilon-\cos\mu}{1-(1-\epsilon)\cos\mu} = \frac{1}{N}\frac{-\epsilon + \mu^2/2 + O(\mu^4)}{\epsilon + \mu^2/2 + O(\epsilon\mu^2, \mu^4)}.$$

Fix ϵ and change μ. As we pass near the singularity, the term tends to $-1/N$ (when $\mu = 0$). Sufficiently far from the singularity, the value of the term is $+1/N$.

Now we derive a condition that ensures that the vector field has non-zero index on the circle $\gamma = 1-\epsilon$, $\epsilon \to 0+$. (By a standard theorem [35], this will immediately imply the existence of a fixed point inside, as desired.) Specifically, we would like V_γ to be positive everywhere on the circle, so that the the vector field always points outward. Consider the contributions of the various terms to the index. If $\theta_1, \cdots, \theta_N$ are all distinct, then even though the kth term in the sum for V_γ becomes $-1/N$, the other $(N-1)$ terms are all $+1/N$, hence V_γ remains positive. When two θ's are identical, two terms in V_γ become $-1/N$ at the corresponding singularity so that V_γ becomes non-positive unless there are at least three other θ's with different phases from the two. More

generally, one can see that V_γ stays positive all over the circle if and only if the largest group of identical θ's (the largest "cluster") contains less than half of the oscillators.

From now on, suppose that the size of the largest cluster is less than $N/2$, so that V_γ is positive everywhere on the circle. Then, since V_Θ is well-behaved everywhere on $\gamma = 1 - \epsilon$, the vector field always points outward. Hence the index along the circle is $+1$. We conclude that the vector field must have at least one fixed point inside the disk. The coordinates of this fixed point are the desired solution (Θ, γ) of (4.16).

Once we obtain Θ and γ at the solution, these values are substituted in (3.2) to obtain N equations for Ψ and $\{\psi_j\}$. Another, somewhat arbitrary, constraint on $\{\psi_j\}$ can be imposed at this moment to determine Ψ uniquely. One candidate is

$$\sum_{k=1}^{N} \psi_k = 0. \tag{4.17}$$

This constraint picks one incoherent set of $\{\psi_j\}$ from others that differ only by a rigid rotation. Solving (3.2) for ψ_j and substituting it into (4.17), we obtain

$$\sum_{k=1}^{N} \left[\Psi + 2 \arctan\left(\sqrt{\frac{1-\gamma}{1+\gamma}} \tan[\tfrac{1}{2}(\theta_k - \Theta)] \right) \right] = 0 \tag{4.18}$$

which determines Ψ. Finally, $\{\psi_j\}$ is obtained from (3.2). Thus the conversion is complete. This concludes the proof of the lemma. □

Remarks

(1) The fixed point guaranteed by the lemma seems to be *unique*. Numerical evidence for this conjecture is presented in the subsection after the next. We have been unable to find a proof of the uniqueness.

(2) The lemma fails for states that contain majority ($\geq N/2$) clusters. It turns out that these states are incompatible with the incoherence condition (4.12). To understand why the failure occurs, regard the transformation (3.2) as a reparametrization of the unit circle, mapping ψ_j to θ_j. The circle is stretched in some places and shrunken in others, but the ordering and topology of the oscillators are preserved. For almost all configurations $\{\theta_j\}$, this reparametrization can successfully produce a preimage $\{\psi_j\}$ with its centroid at the origin. However, when there is a cluster containing at least $N/2$ oscillators, the centroid cannot possibly vanish; even if all the remaining oscillators are pushed diametrically opposite the cluster, they still cannot counterbalance it. Hence, there is no hope of expressing such a state in terms of an incoherent preimage.

(3) Although our method of parametrizing the $\{\theta_j\}$ by incoherent $\{\psi_j\}$ was suggested by the particular form of the averaged system (4.4), the method has nothing to do with the evolution equations themselves. The same conversion works for other reducible equations of the form (3.1).

4.2.4. *Potential function*

The expressions V_Θ and V_γ defined in (4.16) seem to be partial derivatives of some function, just as the sums in (4.4) were partial derivatives of a function $\mathcal{H}$. This analogy is, of course, due to the invariance of (3.2) with respect to the exchanges (4.14). It is easy to see that if we define a function

$$\mathcal{U}(\Theta,\gamma) = \frac{1}{N}\sum_{k=1}^{N}\log\left(\frac{1+\gamma\cos(\theta_k-\Theta)}{\sqrt{1-\gamma^2}}\right) \tag{4.19}$$

corresponding to $\mathcal{H}$ in (4.5), then we obtain formulas corresponding to (4.6) and (4.7), namely

$$\frac{\partial\mathcal{U}}{\partial\Theta} = \frac{1}{N}\sum_{k=1}^{N}\frac{\gamma\sin(\theta_k-\Theta)}{1+\gamma\cos(\theta_k-\Theta)} = V_\Theta\,,$$

$$\frac{\partial\mathcal{U}}{\partial\gamma} = \frac{1}{N(1-\gamma^2)}\sum_{k=1}^{N}\frac{\gamma+\cos(\theta_k-\Theta)}{1+\gamma\cos(\theta_k-\Theta)} = \frac{V_\gamma}{1-\gamma^2}\,, \tag{4.20}$$

where $0 \le \gamma < 1$, as before. Fixed points of (4.16) correspond precisely to stationary points of $\mathcal{U}$. The vector $(V_\Theta/\gamma, V_\gamma/(1-\gamma^2))$ points in the direction of steepest ascent on the potential function $\mathcal{U}$.

The functions $\mathcal{H}$ and $\mathcal{U}$ are strikingly similar. In fact, they differ only by a sign. To see this, use the first equation of (3.3) to express $\mathcal{H}$ in (4.5) as

$$\mathcal{H} = \frac{1}{N}\sum_{k=1}^{N}\log\left(\frac{\sin(\psi_k-\Psi)}{\sin(\theta_k-\Theta)}\right). \tag{4.21}$$

Using the symmetric counterpart (4.15), $\mathcal{U}$ in (4.19) becomes

$$\mathcal{U} = \frac{1}{N}\sum_{k=1}^{N}\log\left(\frac{\sin(\theta_k-\Theta)}{\sin(\psi_k-\Psi)}\right). \tag{4.22}$$

Therefore,

$$\mathcal{U}(\Theta,\gamma;\{\theta_j\}) = -\mathcal{H}(\Psi,\gamma;\{\psi_j\})\,. \tag{4.23}$$

Another interesting relation between the two functions is that $\mathcal{U}$ can be regarded as $\mathcal{H}$ via the transformation

$$\mathcal{U}\to\mathcal{H}, \quad \gamma\to\gamma, \quad \theta_j\to\psi_j, \quad \Theta\to\Psi\pm\pi\,. \tag{4.24}$$

Thus if the given data sets, $\{\theta_j\}$ for $\mathcal{U}$ and $\{\psi_j\}$ for $\mathcal{H}$, are the same, then $\mathcal{U}$ at (Θ,γ) gives the same value as $\mathcal{H}$ at $(\Psi\pm\pi,\gamma)$. This is useful when we draw contour curves of both functions and study their surfaces.

4.2.5. Numerical conversion of initial conditions

We have not found an explicit analytical expression for the solution (γ,Θ) of (4.16). Computing it numerically, however, is not difficult. The following procedure has worked for all the cases we have tested, and we conjecture that it is valid in general.

For all initial conditions $\{\theta_j\}$ without a majority cluster, the potential $\mathcal{U}$ is found numerically to have a *unique* minimum within $0 \le \gamma < 1$. The minimum can be reached from a suitable starting point by following, for example, the steepest descent path.

To facilitate intuition, we plot typical contour curves of $\mathcal{U}$ in Fig. 6, for $N = 8$. The values of $\theta_1,\ldots,\theta_8$ are indicated by dots on the unit circle; the numbers attached to them indicate the multiplicity of phases at that point. In Fig. 6 there is one cluster of size two, and six isolated

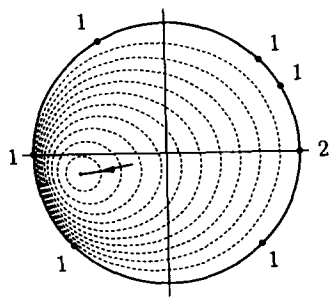

Fig. 6

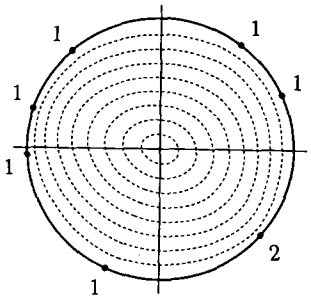

Fig. 7

Fig. 6. A typical contour of $\mathcal{U}$, plotted on the plane with polar coordinates γ and Θ, and assuming there is no majority cluster. The dots on the unit circle represent the phases θ_j, given as parameters. The numbers attached to the dots denote multiplicities. There are $N = 8$ oscillators. The values of θ_j are: π, $2\pi/3$, $\pi/4$, $\pi/6$, 0 (double), $-\pi/4$, and $-3\pi/4$. The level curves are closed and off-centered. The minimum can be easily computed; the solid line is the steepest descent path obtained numerically.

Fig. 7. A typical contour of $\mathcal{H}$, plotted on the plane with polar coordinates γ and Ψ. The incoherent conversion of initial conditions is used. The dots represent the preimages ψ_j computed for the θ_j given in Fig. 6. The centroid of ψ_j is at the origin. The function $\mathcal{H}$ is convex, with its minimum at the origin.

oscillators. The contours of $\mathcal{U}$ (dashed closed curves) decrease monotonically from a maximum near $\gamma = 1$, where $\mathcal{U}$ is large and positive, to a minimum at the innermost contour. This is the stationary point we would like to compute.

The minimum is typically located opposite the centroid of the oscillators with respect to the origin. Hence, $\gamma = R$ and $\Theta = \phi \pm \pi$ is a good initial guess of the location. Integrating along the steepest descent direction from this guess, the path (shown in Fig. 6 as a solid curve) converges to the minimum. The coordinates (γ, Θ) of the minimum yield the initial conditions for the system (4.4) (or other reduced equations), and the minimum value of $\mathcal{U}$ gives the initial value of $-\mathcal{H}$. Recall that this quantity will be conserved in the averaged system with $\sin\delta = 0$.

4.3. *The Lyapunov function*

This section resolves the second issue posed at the end of Section 4.1: we clarify the geometric meaning of the Lyapunov function $\mathcal{H}$ of the reduced system. By imposing the incoherence condition (4.12) on the system constants $\{\psi_j\}$, we will see that $\mathcal{H}$ measures the phase coherence of the N oscillators.

4.3.1. *$\mathcal{H}$ with the incoherence constraints*

Recall from (4.7) that

$$\frac{\partial \mathcal{H}}{\partial \gamma} = \frac{F(\Psi,\gamma)}{1-\gamma^2}, \quad \text{where } F(\Psi,\gamma) = \frac{1}{N}\sum_{k=1}^{N} \frac{\gamma - \cos(\psi_k - \Psi)}{1 - \gamma\cos(\psi_k - \Psi)}.$$

Now imposing the constraint (4.12), we obtain

$$F(\Psi, \gamma = 0) = -\frac{1}{N}\sum_{k=1}^{N} \cos(\psi_k - \Psi) = 0.$$

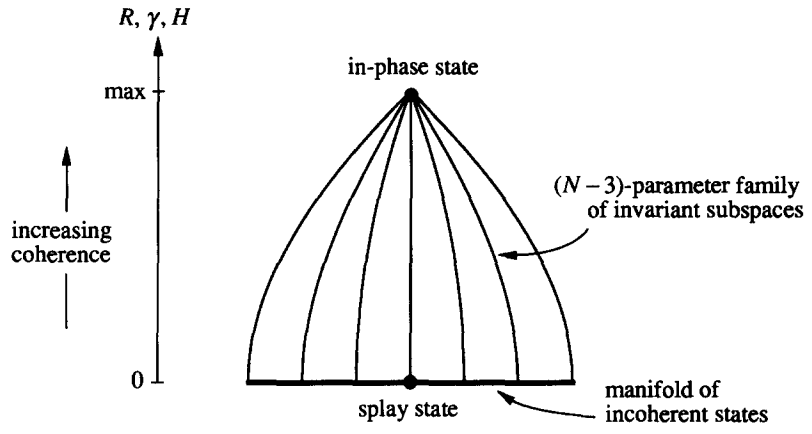

Fig. 8. Foliation of the N-dimensional phase space (schematically) for the averaged systems. Two extreme sets are the in-phase state (maximizing the order parameter R, the distortion parameter γ, and the Hamiltonian $\mathcal{H}$) and the manifold of incoherent states (where R, γ, and $\mathcal{H}$ all vanish). The incoherent states are connected to the in-phase state via an $(N-3)$-parameter family of invariant subspaces, shown as leaves of the foliation.

Thus F and $\mathcal{H}$ vanish on the incoherent manifold.

Moreover, F is strictly increasing in the γ-direction for all Ψ since

$$\frac{\partial F}{\partial \gamma} = \frac{1}{N}\sum_{k=1}^{N} \frac{[1-\gamma\cos(\psi_k-\Psi)]-[\gamma-\cos(\psi_k-\Psi)][-\cos(\psi_k-\Psi)]}{[1-\gamma\cos(\psi_k-\Psi)]^2}$$

$$= \frac{1}{N}\sum_{k=1}^{N} \frac{1-\cos^2(\psi_k-\Psi)}{[1-\gamma\cos(\psi_k-\Psi)]^2} > 0$$

for incoherent $\{\psi_j\}$.

Now adopting radius γ and angle Ψ as the polar variables, the graph of $\mathcal{H}$ becomes a convex well. In this new coordinate system, the contours of $\mathcal{H}$ become concentric curves centered at the *origin*, the minimum of $\mathcal{H}$. Fig. 7 shows typical level curves of $\mathcal{H}$ for $N = 8$. The preimages $\psi_1, \ldots, \psi_8$ satisfying the incoherence constraints are shown as dots, just as the θ's were in Fig. 6.

The function $\mathcal{H}$ has the following properties. From (4.5), $\mathcal{H} = 0$ at $\gamma = 0$. Since F is an increasing positive definite function of γ, $\partial\mathcal{H}/\partial\gamma \to +\infty$ monotonically as $\gamma \to 1$. Moreover, $\mathcal{H}$ itself monotonically increases with respect to γ; in fact, $\mathcal{H} \to \infty$ as $\gamma \to 1$ for any Ψ.

The levels of $\mathcal{H}$ reflect the coherence of the oscillators. For instance, as $\gamma \to 1$, and therefore as $\mathcal{H} \to \infty$, the oscillators are close to the in-phase state. At the other extreme, $\gamma = 0$ and $\mathcal{H} = 0$ implies $\theta_j = \psi_j + (\Theta - \Psi)$, as shown in Section 3.1. In this case $\{\theta_j\}$ becomes the incoherent state $\{\psi_j\}$ itself, only rotated rigidly by the angle $(\Theta - \Psi)$. Hence, the Lyapunov function $\mathcal{H}$ is yet another measure of the phase coherence of the oscillators, as are γ and R.

This interpretation of $\mathcal{H}$ has powerful global implications for the averaged system (4.1). From (4.9), $\dot{\mathcal{H}} = R^2 \sin\delta$. When $\sin\delta > 0$, $\mathcal{H}$ increases in time, and the oscillators approach the in-phase state for almost all initial conditions. When $\sin\delta < 0$, $\mathcal{H}$ decreases, meaning that they spread apart until their centroid vanishes. Thus, the in-phase state is globally attracting when $\sin\delta > 0$, whereas the incoherent manifold is attracting when $\sin\delta < 0$. At the critical value $\sin\delta = 0$, every trajectory runs along a contour of $\mathcal{H}$. As shown above, such contours are closed loops. Each

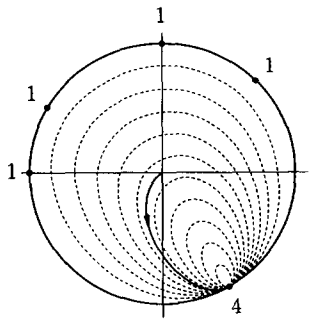

Fig. 9. A typical contour of $\mathcal{H}(\Psi,\gamma)$ when there is a majority cluster of size $N/2$. The dots represent the parameters ψ_j, whose values are: π, $5\pi/6$, $\pi/2$, $\pi/4$, and $-\pi/3$ (multiplicity 4). On the unit circle, $\mathcal{H}$ is infinite everywhere, except at the cluster of four oscillators where it assumes a finite value. The contours are tangent to the circle at the singular point. The solid curve is a computed trajectory of the integrable averaged system ($\delta = 0$). It is not periodic but converges to the singular point. When the cluster size exceeds $N/2$, a similar picture is obtained.

trajectory undergoes periodic motion in the (Ψ,γ) space. In the full phase space, the motion is quasiperiodic on 2-tori, for reasons given in Section 4.1.

Fig. 8 shows a schematic drawing of the N-dimensional phase space. On one side, there is an $(N-3)$-dimensional manifold of incoherent states, the most disordered states of the system. On the opposite side, there is the in-phase state, the most ordered one. There is only one such state although there are many ways to approach it. In fact, each point on the incoherent manifold is connected to the in-phase state through a three-dimensional invariant subspace. Such subspaces are stacked side by side as an $(N-3)$-parameter family, shown in Fig. 8 as a family of curves. The $N-3$ parameters are the $\{\psi_j\}$, subject to the two incoherence constraints (4.12) and the third, arbitrary constraint (4.17). On each invariant subspace, the flow is either toward the in-phase state (if $\sin\delta > 0$), toward the incoherent manifold ($\sin\delta < 0$), or neither ($\sin\delta = 0$). In this last case, the motion is quasiperiodic.

4.3.2. Majority clusters

The analysis in the last section does not apply if there is a majority cluster, i.e., if $N/2$ or more θ's are initially equal. Nevertheless, this (highly exceptional) case can be handled by resorting to the identity conversion (3.7). Recall that the preimage $\{\psi_j\}$ is then taken to be identical to $\{\theta_j(0)\}$, and in return, we restrict attention to the trajectory that starts at $\gamma(0) = \Psi(0) = \Theta(0) = 0$.

When we use the identity conversion, the contours of $\mathcal{H}$ are off-centered like those of $\mathcal{U}$, as described in the preceding section. Indeed, since $\{\psi_j\}$ is now identical to $\{\theta_j\}$, the contour maps for $\mathcal{H}$ and $\mathcal{U}$ are the same after a rotation by 180 degrees, thanks to (4.24).

Fig. 9 shows typical contours of $\mathcal{H}$ for the case where there is a majority cluster. Here, four of the eight oscillators have equal ψ's. The resulting contour map is qualitatively different from Fig. 6 – the critical point occurs on the circle, and all the contours emanate from it. (The contours for larger clusters of size $> N/2$ look similar.)

The change in contours can be explained by a local analysis of $\mathcal{H}$ near $\gamma = 1$. If we rewrite $\mathcal{H}$ in (4.5) as

$$\mathcal{H} = \frac{1}{N}\sum_{k=1}^{N} \log\left[1 - \gamma\cos(\psi_k - \Psi)\right] - \tfrac{1}{2}\log(1-\gamma^2),$$

we see that the asymptotic behavior as $\gamma \to 1$ is determined by the competition of the terms on the right hand side. The second term becomes singular like

$$-\tfrac{1}{2}\log(1-\gamma^2) \sim -\tfrac{1}{2}\log(1-\gamma) \to +\infty \quad \text{as } \gamma \to 1\,.$$

The first term becomes singular at $\gamma = 1$ only when $\Psi = \psi_k$ for some k. Then, the kth term in the sum gives a contribution of

$$\frac{1}{N}\log\left[1-\gamma\cos(\psi_k-\Psi)\right] \sim \frac{1}{N}\log(1-\gamma) \to -\infty \quad \text{as } \gamma \to 1\,.$$

Since the singularities of both terms are $\sim \log(1-\gamma)$, we only need to compare the coefficients. We see that as $\gamma \to 1$,

$$\mathcal{H} \longrightarrow \begin{cases} -\infty & \text{if more than } N/2 \text{ of the } \psi_k \text{ equal } \Psi, \\ \text{finite} & \text{if exactly } N/2 \text{ of the } \psi_k \text{ equal } \Psi, \\ +\infty & \text{otherwise.} \end{cases}$$

Therefore, when there is no majority cluster, $\mathcal{H}$ is $+\infty$ everywhere on the circle $\gamma = 1$. When there is a majority cluster, $\mathcal{H}$ still equals $+\infty$ at all points of the circle *except* at the cluster; there it is either finite or $-\infty$. In this case all contour curves originate from one side of the singular point and return to the other side as in Fig. 9.

To illustrate some of the new effects caused by a majority cluster, consider the trajectories of the averaged system, in the case $\sin\delta = 0$. Recall that when we use the identity conversion, only the trajectory starting from $\gamma(0) = \Psi(0) = 0$ is meaningful. This solution is shown in Fig. 9 as a solid curve. It follows a contour of $\mathcal{H}$ and converges to the singular point on $\gamma = 1$. In contrast to Fig. 6, the trajectory does not execute periodic motion in γ and Ψ, but rather terminates at a cluster state.

4.4. *Visualizing flows*

In this section we present numerical phase portraits of the averaged system (4.1) for $N = 3$ and $N = 4$. We assume $\sin\delta = 0$ unless otherwise stated. Although the essential dynamics can be understood already by the (γ, Ψ)-diagram of the reduced system, it is much more instructive to view the dynamics in the original θ-coordinates. We thereby obtain a picture of the phase space that improves upon the schematic Fig. 8. For instance, the incoherent manifold and the $(N-3)$-parameter family of invariant subspaces can be visualized directly.

Without loss of generality, the permutation symmetry of (4.1) enables the oscillators to be ordered as follows:

$$\theta_N \le \theta_{N-1} \le \ldots \le \theta_2 \le \theta_1 \le \theta_N + 2\pi\,.$$

Eq. (4.1) also implies that if $\theta_i = \theta_j$ at any time, they remain equal forever. Thus $\theta_i = \theta_j$ defines an invariant hyperplane for each (i, j) pair, and the whole phase space is partitioned into invariant cells. The ordering given above defines a "canonical invariant region [21,36]. Trajectories that start in this region are stuck in there forever; in more physical terms, the oscillators can never pass each other as they run around the unit circle.

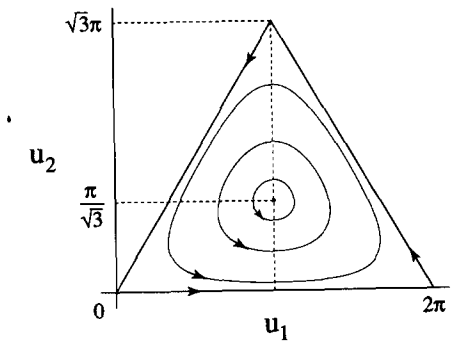

Fig. 10

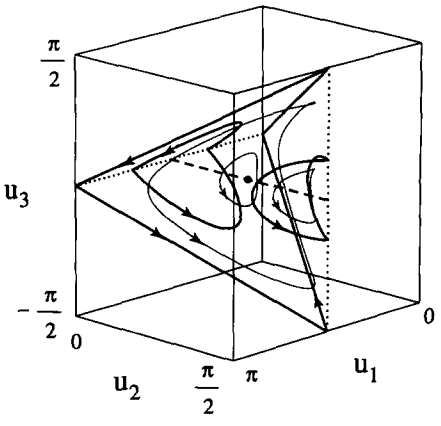

Fig. 11

Fig. 10. Flow of the integrable ($\delta = 0$) averaged system for $N = 3$ in the original coordinates θ_j. The linear transformation $\bar{\theta} = \sum_{j=1}^{3} \theta_j$, $u_1 = \theta_1 - (\theta_2 + \theta_3)/2$, $u_2 = \sqrt{3}(\theta_2 - \theta_3)/2$ is used to bring out the picture's inherent symmetry. The mean phase $\bar{\theta}$ is decoupled, and is not shown. Only one triangular region, corresponding to the ordering $\theta_3 \le \theta_2 \le \theta_1 \le \theta_3 + 2\pi$ is shown since flows in the other regions are equivalent by symmetry. The phase portrait shows a continuous family of periodic orbits circulating around the splay state (dot in the center). If the mean phase direction were restored, the motion would appear as quasiperiodic motion on 2-tori.

Fig. 11. Flow of the integrable ($\delta = 0$) averaged system for $N = 4$ in the original coordinates θ_j. The linear transformation $\bar{\theta} = \sum_{j=1}^{4} \theta_j$, $u_1 = (\theta_1 + \theta_2 - \theta_3 - \theta_4)/4$, $u_{2,3} = (\pm\theta_1 \mp \theta_2 + \theta_3 - \theta_4)/4$ is used. The mean phase $\bar{\theta}$ is decoupled, and is not shown. The tetrahedron is the canonical invariant region, corresponding to the ordering $\theta_4 \le \theta_3 \le \theta_2 \le \theta_1 \le \theta_4 + 2\pi$. Notation: dotted edges of the tetrahedron = two pairs of equal θ's; solid edges = three equal θ's; vertices = in-phase solutions; dashed bar inside = filament of incoherent states; dot at center = splay state. Three thin solid loops inside the region are computed trajectories. Four thick curves forming two closed loops are trajectories on the faces of the tetrahedron, representing clustered configurations of oscillators.

4.4.1. Integrable flow for $N = 3$

Since the right hand side of (4.1) depends only on the phase differences, the mean phase can be removed from the dynamics. For $N = 3$, for example, we may use the linear transformation [2,21]:

$$\bar{\theta} = \tfrac{1}{3}\sum_{k=1}^{3} \theta_k, \quad u_1 = \theta_1 - \tfrac{1}{2}(\theta_2 + \theta_3), \quad u_2 = \tfrac{1}{2}\sqrt{3}(\theta_2 - \theta_3).$$

Since $\bar{\theta}$ is passively driven by the (u_1, u_2) dynamics, it suffices to draw the effective dynamics on the (u_1, u_2)-plane. In Fig. 10, the canonical invariant region $\theta_3 \le \theta_2 \le \theta_1 \le \theta_3 + 2\pi$ appears as a triangle. The sides $u_2 = 0$, $u_1 - u_2/\sqrt{3} = 0$, and $u_1 + u_2/\sqrt{3} = 2\pi$ correspond to $\theta_3 = \theta_2$, $\theta_2 = \theta_1$, and $\theta_1 = \theta_3 + 2\pi$, respectively. The vertices all correspond to the in-phase state $\theta_1 = \theta_2 = \theta_3 \pmod{2\pi}$. There are three ways to approach the in-phase state while maintaining the order of the three oscillators. Since the $\bar{\theta}$-direction is projected out, the periodic solutions look like fixed points.

The dot in the center of the triangle is the splay state

$$\theta_1(t) = \theta_2(t) + \tfrac{2}{3}\pi = \theta_3(t) + \tfrac{4}{3}\pi \quad \text{for all } t.$$

It satisfies the incoherence conditions (4.11), and being periodic, it also appears as a fixed point in the figure.

Through the transformation (3.2) and the three constraints (4.12) and (4.17), we must obtain

$$\psi_1 = \tfrac{2}{3}\pi, \quad \psi_2 = 0, \quad \psi_3 = -\tfrac{2}{3}\pi$$

from almost all initial conditions. This is the preimage of the oscillators. Generic trajectories form concentric loops around the splay state. Each trajectory is indeed on a 2-torus when the $\bar{\theta}$-direction is reinstated.

On the edges of the triangle, two of the oscillators are in phase. Because the size of this cluster exceeds $N/2$, the initial conditions cannot be converted to the splay phase preimage. The edges of the triangle are separatrices (separating neighboring canonical invariant regions corresponding to different choices of the ordering), and the behavior differs qualitatively from the generic case. From Fig. 10 we see that trajectories on the edges are attracted toward the vertices. Starting from one isolated oscillator and a cluster of two others, they eventually merge to form a cluster of three, i.e. they approach the in-phase state. On the separatrices, the motion is not quasiperiodic, but rather appears to have a dissipative character.

4.4.2. Integrable flow for $N = 4$

Since $\bar{\theta}$ can be projected out, we may display the phase portrait for $N = 4$ in three dimensions. This turns out very helpful. The dimension of the incoherent manifold becomes $N - 3 = 1$, which is not trivial as it was for $N = 3$.

As pointed out by Tsang and Schwartz [2], a nice transformation in this case is

$$\bar{\theta} = \tfrac{1}{4}\sum_{k=1}^{4}\theta_k, \quad u_1 = \tfrac{1}{4}(\theta_1 + \theta_2 - \theta_3 - \theta_4), \quad u_{2,3} = \tfrac{1}{4}(\pm\theta_1 \mp \theta_2 + \theta_3 - \theta_4).$$

Fig. 11 shows the projection of the canonical invariant region

$$\theta_4 \le \theta_3 \le \theta_2 \le \theta_1 \le \theta_4 + 2\pi$$

onto the (u_1, u_2, u_3)-space. The four side walls of the tetrahedron $u_2 + u_3 = 0$, $u_1 - u_2 = 0$, $u_2 - u_3 = 0$, and $u_1 + u_2 = \pi$ correspond to $\theta_4 = \theta_3$, $\theta_3 = \theta_2$, $\theta_2 = \theta_1$, and $\theta_1 = \theta_4 + 2\pi$, respectively. There are six edges. Four of them, shown in the figure as solid lines, correspond to three identically phased θ's (the 3+1 states). Two other edges, shown as dotted lines, are two pairs of equal θ's (the 2+2 states). As can be easily checked from (4.1), the points on the 2+2 edges are fixed (meaning the solutions are periodic when $\bar{\theta}$ is reinstated). The four vertices, also shown as fixed points, all correspond to the in-phase solution as before. There are four ways to approach the in-phase state while staying in the canonical invariant region.

There is a dashed bar inside the tetrahedron, connecting the 2+2 edges. It is the one-dimensional *manifold of incoherent states*. Each point on this bar appears fixed since the incoherent states are periodic solutions of (4.1). The dot in the middle of the incoherent manifold is the splay-phase solution, i.e., four oscillators with equally spaced phases.

Generic trajectories are shown as thin solid curves inside the region. They are periodic in the figure, meaning quasiperiodic when $\bar{\theta}$ is included. Trajectories close to the splay state oscillate around the incoherent bar in an almost circular fashion. Trajectories far from the bar are strongly distorted. One large loop shown in the figure visits all four corners closely. The trajectory is slow near corners, and runs rapidly in between. This motion describes the situation when four oscillators are almost in-phase, but one of them suddenly departs from the other three, rotates once, and reapproaches the group. Such "phase slips" appear for any N when a trajectory is close to the in-phase solution. Phase slips also occur for most trajectories when $\sin\delta > 0$ (in-phase is attracting)

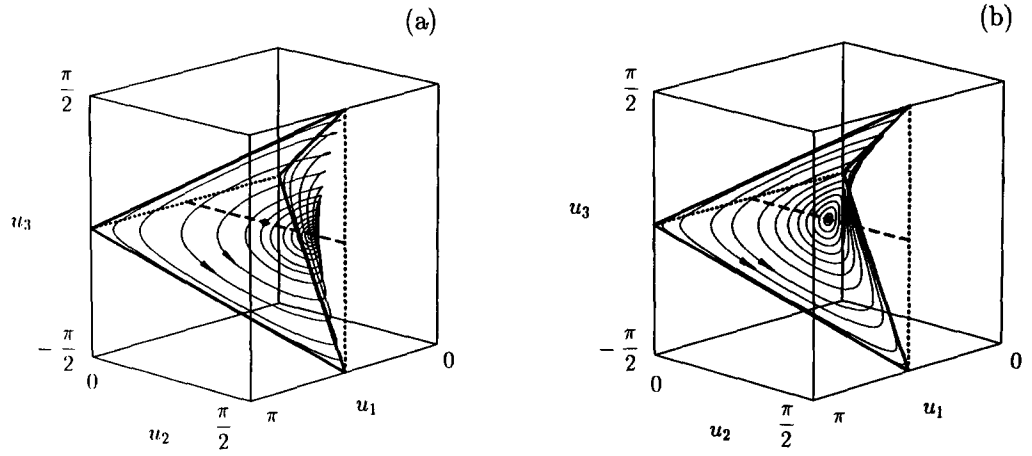

Fig. 12. Trajectories of the integrable flow for $N = 4$, corresponding to a particular preimage $\{\psi_j\}$. The reduced equations (4.4) with $\delta = 0$ are integrated from $\Psi(0) = \Theta(0) = 0$ and various values of $\gamma(0)$. For each $\gamma(0)$, the trajectory is a closed orbit. As $\gamma(0)$ varies, the orbits sweep out a warped surface. The surface intersects the incoherent filament transversely. Changing $\{\psi_j\}$ moves this intersection along the filament.
(a) $\psi_{1,4} = \pm 9\pi/10$, $\psi_{2,3} = \pm\pi/10$. (b) $\psi_{1,4} = \pm 3\pi/4$, $\psi_{2,3} = \pm\pi/4$. This choice of $\{\psi_j\}$ yields the most symmetric possible surface. It emanates from the splay state (solid dot at center).

if we wait for a long time. In this case, the time between slips becomes unbounded as a trajectory approaches the in-phase state.

The four thick curves (forming two closed loops) in Fig. 11 are trajectories on the boundary walls of the tetrahedron, meaning a pair of θ's are identically phased. This is when the size of the largest cluster is exactly $N/2$. The flow is toward the $2+2$ edges, and must end up there. Non-paired oscillators come together to form a cluster that competes with the paired ones.

On the $3+1$ edges (four solid lines) the flow is directed toward the vertices, i.e., the in-phase state. Thus the flow on the separatrix is similar to that of Fig. 4.5; once again, quasiperiodic motion does not occur if there is a sufficiently large cluster.

4.4.3. Invariant subspaces

For $N = 4$, we can visualize the $(N-3)$-parameter family of three-dimensional subspaces. If $\bar{\theta}$ is projected out, then Θ is eliminated from the phase portrait. (Note that $\theta_i - \theta_j$ does not involve Θ.) Thus we should see a one-parameter family of two-dimensional surfaces foliating the interior of the tetrahedron. The sole parameter is the location of the surface along the incoherent manifold.

One such surface is computed and shown in Fig. 12a. We chose a set of $\{\psi_j\}$ satisfying the three constraints. The reduced equations (4.4) were then integrated numerically from $\Theta(0) = \Psi(0) = 0$ (without loss of generality), for various values of $\gamma(0)$. Next the transformation (3.2) was applied to the results to recover $\{\theta_j(t)\}$. Finally these phases were themselves converted to the phase differences (u_1, u_2, u_3) shown in Fig. 12a.

When $\gamma(0) = 0$, the trajectory is confined to the incoherent manifold. As $\gamma(0)$ is increased, the orbits sweep out a warped surface, as expected. Each trajectory is periodic. (These closed orbits correspond to invariant 2-tori in the full phase space, after we reinstate $\bar{\theta}$.)

A different choice of $\{\psi_j\}$ would produce another surface. In particular, $\psi_{1,4} = \pm 3\pi/4, \psi_{2,3} = \pm\pi/4$ (evenly spaced oscillators as the preimage) produces a symmetric surface emanating from the splay-phase dot (Fig. 12b). The two principal curvatures of this surface at the splay state have

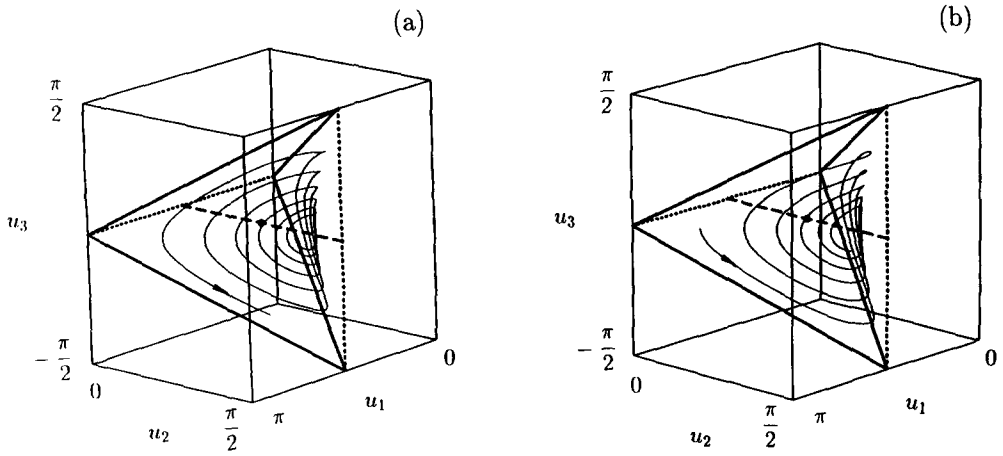

Fig. 13. Trajectories of the averaged system with $\delta \neq 0$. In contrast to Fig. 12, the trajectories are spirals, not closed orbits. However, they still lie on the same warped surface as in Fig. 12, since this surface is determined solely by $\{\psi_j\}$, and the same ψ's as used as in Fig. 12a.
(a) Outward spiral: $\delta = +\pi/100$, $\gamma(0) = 0.5$, $\Psi(0) = \Theta(0) = 0$. (b) Inward spiral: $\delta = -\pi/100$, $\gamma(0) = 0.99$, $\Psi(0) = \Theta(0) = 0$.

the same magnitude.

These membrane-like surfaces are neatly stacked side by side, skewered by the incoherent filament. On each surface the dynamics are governed by a one degree of freedom Hamiltonian system. Note that the "frame" of the membrane surfaces, i.e., the limiting trajectory as $\gamma \to 1$, is formed by the four edges of the 3+1 states, joined at the in-phase vertices.

We now have a global picture of phase space that improves on the earlier schematic Fig. 8. The warped surfaces of Figs. 12a and b correspond to the curves that connect the in-phase state to the incoherent manifold in Fig. 8. The in-phase dot in Fig. 8 should be represented, more precisely, by the whole frame of the 3+1 edges of Fig. 12.

There is also a correspondence between Figs. 10 and 12: if we flatten any of the warped surfaces of Fig. 12, we obtain a picture similar to Fig. 10. In both cases, a continuous family of closed curves is bounded by a polygon; only the number of vertices is increased. Trajectories near the polygonal frame slow down near the vertices and run rapidly in between. They generally have N phase-slips before completing a period of the (Ψ, γ)-dynamics.

We conclude with two examples where $\sin\delta \neq 0$; then $\mathcal{H}$ is no longer conserved. Fig. 13a plots a representative trajectory for the case $\delta = +\pi/100$. For this case, $\mathcal{H}$ is a monotonically increasing function of time, and the trajectory spirals out to the in-phase state. The trajectory is, however, confined to the same warped surface as in Fig. 12a since this surface is determined by $\{\psi_j\}$, and the same $\{\psi_j\}$ have been used in both figures. Fig. 13b shows the case $\delta = -\pi/100$. Now the trajectory spirals down to the incoherent filament, and approaches a final state predetermined by the $\{\psi_j\}$.

4.5. Origin of degeneracy

4.5.1. Degeneracy of averaged systems

There are three levels of degeneracy exhibited by the averaged system (4.2). We discuss them in order of increasing specialization.

First, the whole phase space has a cellular structure, made up of identically-shaped invariant

regions. The flows inside all the cells are equivalent. These properties follow from the permutation symmetry of the system.

Second, each N-dimensional cell is itself partitioned into three-dimensional invariant subspaces. This partitioning occurs for all "reducible" systems of the form (3.1); the averaged system (4.1) belongs to this subclass. This level of degeneracy is due to the absence of explicit higher harmonics in (3.1). The transformation (3.2) works in this case, and converts the N-dimensional system to the reduced three-dimensional system for (γ, Ψ, Θ). Nevertheless, the reduced dynamics can be rich: there can be fixed points, periodic solutions, chaos, coexistence of dissipative and conservative behaviors, etc.

Third, the averaged system (4.1) is more special than other reducible systems because it possesses a rotational invariance – it depends only on the phase differences of the oscillators, not on the phases themselves. When we apply the transformation (3.2) to the averaged system, the variable Θ is canceled upon taking phase differences, and so the right hand sides of (4.1) depend only on γ and Ψ. Thus the averaged system has effectively two-dimensional dynamics, and chaos is therefore impossible.

It is interesting that the effective system turned out to have a Lyapunov function whose properties were independent of $\{\psi_j\}$. This enabled the averaged system to be thoroughly analyzed. Along the way, we found it useful to constrain the $\{\psi_j\}$ to be incoherent. These constraints associated $\gamma = 0$, or equivalently $\mathcal{H} = 0$, with the manifold of incoherent states. Notice that this association was not mandatory; we might have chosen $\gamma = 0$ to label some other states by imposing different constraints. However, the "core" of dynamics of the averaged system happened to be the incoherent manifold, so our choice seemed natural. In particular, given that the incoherent states are stationary under the flow (4.1), it seemed sensible to tailor the coordinate system (Ψ, γ) around them. This explains why we didn't need to resort to Cartesian expressions when analyzing the averaged systems.

4.5.2. *Surviving structure in non-averaged systems*

Many of the results obtained for averaged systems carry over to more general reducible systems, including Josephson arrays. The main difference is that general systems are not rotationally invariant; Θ no longer disappears from the right hand sides of the reduced equations. Thus the reduced system is now three-dimensional, not two-dimensional.

Furthermore, the incoherent states are no longer stationary, and the coordinate system cannot be tailored to the flow. In particular, the states with $\gamma = 0$ are no longer fixed. To avoid a coordinate singularity, we must resort to a Cartesian-type coordinate system, as described in Section 3.1.

However, the conversion of initial conditions is unaffected. The best approach is still to impose the three constraints (4.12) and (4.17) on a set of constants $\{\psi_j\}$. One set of $\{\psi_j\}$ corresponds to a particular three-dimensional subspace. Thus the trajectories of all reducible systems are confined to the same subspaces as before – only the evolution inside the subspaces is different, and depends on the governing equations.

4.5.3. *Explaining previous observations*

Our results shed some light on the observations listed in Section 2.4.

Observation 1 (existence of at least $N - 2$ neutrally stable directions around the splay state) is now proven. The results of Section 3.2 hinted that this observation was somehow related to reducibility, but it was not clear how different subspaces were related to one another. We now see

that the neutral stability follows from the foliation of phase space by an $(N-3)$-parameter family of invariant subspaces: $N-3$ neutral directions correspond to perturbations from one subspace to another, and one additional direction corresponds to trivial perturbations along the splay-phase orbit itself.

Then why doesn't the in-phase periodic solution exhibit a similar degeneracy? Because (as shown in Section 4.4) the in-phase solution lies at the "hinge" of the foliation where all the subspaces meet, it is meaningless to speak of perturbations across subspaces at this point, and so the in-phase state can be attracting, at least in some cases.

Although Observation 1 was originally suggested by numerical experiments on the splay state, it is now clear that the same statement holds for *all* incoherent periodic states (if they exist). Moreover, even for arbitrary, non-periodic trajectories, we may conclude that there are at least $N-3$ Lyapunov exponents equal to zero.

The status of Observation 2 (foliation by invariant 2-tori for resistively loaded arrays) is more problematic. We have proven that Observation 2 is correct in the weak-coupling limit – the averaged equations then have $\delta = 0$ and the Hamiltonian $\mathcal{H}$ provides an additional constant of motion, yielding complete integrability and the desired foliation by 2-tori. But for the case of stronger coupling, Observation 2 is probably false, strictly speaking, because the tori seem to break as the coupling increases. Nevertheless, a family of invariant 2-tori might persist near the splay state; perhaps this issue can be settled using KAM theory for reversible systems [31].

Observation 3 (the existence of a manifold of incoherent periodic states) is the most problematic of all. Such a manifold certainly exists in the weak-coupling limit. It is attracting, repelling, or neutral depending on δ, and it organizes the dynamics of the averaged system. But its existence in general is an open problem. In the next subsection we present some tentative ideas on this topic.

4.5.4. *Persistence of incoherent manifold*

Numerical results suggest that a manifold of incoherent periodic states persists if the coupling is not weak, and that such manifold exists for certain Josephson arrays as well. Using the reduction method, we may outline a strategy for an existence proof, at least for the resistively loaded array and for a certain parameter range, as follows.

The reduced equations are (3.17). Numerics suggest (but this is not proven) that for an appropriate range of parameters, the disc $x^2 + y^2 < 1$ at $\Phi = 0$ is mapped into itself at $\Phi = 2\pi$. Since the flow in between is continuous, Brouwer's fixed point theorem implies that the map of the disc to itself has a fixed point, corresponding to a solution of the flow that is 2π-periodic in Φ. From (3.2) it is clear that all θ_j advance by 2π when Φ advances by that amount, and x and y return to their original values. Hence the fixed point of the map corresponds to a time-periodic solution of the array equations.

This argument holds regardless of $\{\psi_j\}$, as long as the map is well-defined. Thus each subspace contains an incoherent periodic solution. (Strictly speaking, the centroid does not vanish for these solutions. However, the word "incoherent" should not be confusing.) Changing $\{\psi_j\}$ continuously, we generate a manifold of incoherent periodic states.

It will be interesting to see if this heuristic argument can be made rigorous.

5. Continuum limit

This section deals with the infinite-N limit of the reducible system (3.1). For series arrays of Josephson junctions, N is typically on the order of 10^3. Thus, the continuum limit is a reasonable approximation. However, our main interest is theoretical: the continuum limit gives rise to an integro-partial differential equation with low-dimensional effective dynamics as well as interesting soliton-like solutions.

For finite N, the dependent variables are the phases $\theta_1, \ldots, \theta_N$, visualized as particles moving on the unit circle. In continuum limit we are less interested in this Lagrangian view. Instead, we concern ourselves with the *density* $\rho(\theta, t)$ of oscillators at a given angle θ at time t. It satisfies the normalization constraint

$$\oint_{-\pi}^{\pi} \rho(\theta, t) d\theta = 1 \quad \text{for all } t. \tag{5.1}$$

Each oscillator is now viewed as a constituent particle of a "fluid". The density function, therefore, obeys the conservation law

$$\frac{\partial \rho}{\partial t} + \frac{\partial}{\partial \theta}(\rho v) = 0, \tag{5.2}$$

where $v(\theta, t)$ is the velocity field. The appropriate v must be the generalization of the velocity of an individual oscillator in the finite-N case, given by (3.1). Thus, taking $N \to \infty$, v is given by

$$v(\theta, t) = f + g \cos\theta + h \sin\theta, \tag{5.3}$$

where f, g, h are functions of time t. Eq. (5.2) with (5.3) is the governing equation for the oscillator density ρ. (The finite-N equations can be recovered by taking the density function ρ to be a sum of δ-functions and by considering the characteristics of (5.2).) We are now asked to solve this kinematic wave problem posed on a periodic domain.

Usually, waves in a periodic domain are analyzed by decomposition into Fourier modes and then considering interactions among the modes. However, since we have already analyzed the finite-N version, we only need to extend our reduction method to the infinite-N equation. In Section 5.1, we show that the partial differential equation (5.2) can be reduced to just three ordinary differential equations. Section 5.2 analyzes the averaged equations for this system, obtained in the weak-coupling limit. Then the effective dynamics become two-dimensional, and a Lyapunov function and global stability results can be obtained.

Eqs. (5.2, 5.3) can be viewed as one of the rare examples of an infinite-dimensional evolution equation whose dynamical complexity is rigorously bounded. It can produce at most three-dimensional chaos, as well as quasiperiodicity on 2-tori, depending on the functions f, g, and h. For one special case (Section 5.3) the system becomes completely integrable, and solitons are observed as in other integrable systems. Finally, Section 5.4 shows some illustrative numerical examples of solitary waves, chaos, and wave interactions.

5.1. General reducible systems

5.1.1. Reduction

The reduction of the continuity equation (5.2) with (5.3) is based on the same idea as the reduction of the finite-N equations (3.1). However, the details differ slightly, and are described here for completeness.

The main idea is to reduce (5.2) via a time-dependent change of coordinates from θ to ψ, using (3.2):

$$\tan[\tfrac{1}{2}(\theta - \Theta(t))] = \sqrt{\frac{1+\gamma(t)}{1-\gamma(t)}}\tan[\tfrac{1}{2}(\psi - \Psi(t))]. \tag{5.4}$$

The claim is that the time-dependent density $\rho(\theta,t)$ will transform into a *stationary* density $\sigma(\psi)$ if (γ,Ψ,Θ) satisfy appropriate ordinary differential equations, to be determined. The two densities are related by:

$$\rho(\theta,t)d\theta = \sigma(\psi)d\psi \qquad \text{for all } t, \tag{5.5}$$

to conserve oscillators in any infinitesimal interval.

We organize the necessary formulas. First, (3.3, 3.4) can be used just by reading θ_j as θ and ψ_j as ψ. The symmetric counterpart of (3.3) is (4.15), which can be used in the same manner. Now, solve (5.4) with respect to ψ to obtain

$$\psi = \Psi(t) + 2\arctan(\Gamma(t)^{-1}\tan[\tfrac{1}{2}(\theta - \Theta(t))]), \tag{5.6}$$

where $\Gamma = \sqrt{(1+\gamma)/(1-\gamma)}$ as in Section 3.1. Following the strategy used to derive (3.5), we obtain

$$\frac{\partial\psi}{\partial t} = \dot{\Psi} - \frac{\dot{\gamma}}{1-\gamma^2}\sin(\psi - \Psi) - \frac{1-\gamma\cos(\psi-\Psi)}{\sqrt{1-\gamma^2}}\dot{\Theta}. \tag{5.7}$$

(This relation can be also obtained from (3.5) by considering the symmetry (4.14).) From (5.6) one finds

$$\frac{\partial\psi}{\partial\theta} = \frac{1-\gamma\cos(\psi-\Psi)}{\sqrt{1-\gamma^2}}. \tag{5.8}$$

Using these formulas, (5.2),(5.3) can be expressed in terms of the new coordinate ψ. In Appendix A we show that the continuity equation can be satisfied identically, regardless of $\sigma(\psi)$, by imposing the three equations:

$$\begin{aligned}
\dot{\gamma} &= -(1-\gamma^2)(g\sin\Theta - h\cos\Theta),\\
\gamma\dot{\Psi} &= -\sqrt{1-\gamma^2}(g\cos\Theta + h\sin\Theta),\\
\gamma\dot{\Theta} &= \gamma f - g\cos\Theta - h\sin\Theta,
\end{aligned} \tag{5.9}$$

which are identical to the reduced equations (3.6) for the finite-N system.

Thus the infinite-dimensional system (5.2, 5.3) is reduced to a system of three ordinary differential equations for (γ,Ψ,Θ). The reduced system involves a time-independent function $\sigma(\psi)$ *as a parameter.*

5.1.2. Converting initial conditions

Given an initial density $\rho(\theta,0) = \rho_0(\theta)$, one can determine initial conditions for the reduced variables $\gamma(0)$, $\Psi(0)$, and $\Theta(0)$, as well as the stationary (preimage) distribution $\sigma(\psi)$. As in the finite-N case, we could use the identity conversion

$$\gamma(0) = \Psi(0) = \Theta(0) = 0 \quad (\text{so, } \theta = \psi), \qquad \sigma(\psi) = \rho_0(\theta). \tag{5.10}$$

A better approach is to parametrize by the incoherent states of the averaged system (shown in Section 5.2). We impose three constraints on $\sigma(\psi)$, analogous to (4.12) and (4.17):

$$\oint \sigma(\psi)\cos\psi d\psi = \oint \sigma(\psi)\sin\psi d\psi = \int_{\Psi-\pi}^{\Psi+\pi} \sigma(\psi)\psi d\psi = 0. \tag{5.11}$$

The range of integration $[\Psi-\pi, \Psi+\pi]$ (in the last relation) is chosen so that $\Psi(0)$ can later be computed easily. The normalization (5.1) yields an additional constraint

$$\oint \sigma(\psi)d\psi = 1. \tag{5.12}$$

To use the parametrization by incoherent states, we need to prove that we can find an incoherent preimage $\sigma(\psi)$ as well as initial conditions $\gamma(0), \Psi(0), \Theta(0)$, given an arbitrary initial condition $\rho_0(\theta)$. The index argument in Section 4.2 goes through with little modification, with the usual caveat that $\rho_0(\theta)$ must not have a "majority cluster", i.e., a δ-spike that contains at least half of the oscillators. Once we find (Θ,γ) for $\rho_0(\theta)$, then Ψ and $\sigma(\psi)$ can be determined from (5.11) and (5.5).

Specifically, (γ,Θ) is obtained as the root of the first two equations of (5.11), rewritten as:

$$\oint \frac{\gamma\sin(\theta-\Theta)}{1+\gamma\cos(\theta-\Theta)}\rho_0(\theta)d\theta = \oint \frac{\gamma+\cos(\theta-\Theta)}{1+\gamma\cos(\theta-\Theta)}\rho_0(\theta)d\theta = 0, \tag{5.13}$$

which comes from a potential function

$$U(\Theta,\gamma) = \oint \log\left(\frac{1+\gamma\cos(\theta-\Theta)}{\sqrt{1-\gamma^2}}\right)\rho_0(\theta)d\theta. \tag{5.14}$$

Then Ψ is given by the third equation of (5.11), written as

$$\int_{\Theta-\pi}^{\Theta+\pi}\left[\Psi + 2\arctan\left(\sqrt{\frac{1-\gamma}{1+\gamma}}\tan[\tfrac{1}{2}(\theta-\Theta)]\right)\right]\rho_0(\theta)d\theta = 0, \tag{5.15}$$

since $\theta \in [\Theta-\pi, \Theta+\pi]$ corresponds to $\psi \in [\Psi-\pi, \Psi+\pi]$. Lastly, the incoherent density preimage $\sigma(\psi)$ is

$$\sigma(\psi) = \rho_0(\theta)\frac{\partial\theta}{\partial\psi} = \rho_0(\theta)\frac{1+\gamma\cos(\theta-\Theta)}{\sqrt{1-\gamma^2}}. \tag{5.16}$$

For any $\sigma(\psi)$ satisfying (5.11) and (5.12), we may associate a three-dimensional set of trajectories by changing γ, Ψ, and Θ over their full ranges. Since infinitely many such $\sigma(\psi)$ can be found, the phase space of (5.2) with (5.3) is foliated by an infinite-parameter family of three-dimensional subspaces. (Recall there used to be $N-3$ parameters for the finite-N systems.) The density $\sigma(\psi)$ characterizes the subspaces.

5.2. Averaged system

It is expected that (5.9) is too hard to analyze in general, so we focus on the averaged system obtained in the weak-coupling limit.

5.2.1. Reduction

Taking the limit $N \to \infty$ of the finite-N averaged system (4.2), we obtain (5.2) and (5.3) with

$$f = 0, \quad g = \oint \rho(\theta,t)\cos(\theta-\delta)d\theta, \quad h = \oint \rho(\theta,t)\sin(\theta-\delta)d\theta. \tag{5.17}$$

Substitution of these expressions into (5.9) gives the reduced equations

$$\frac{\dot\gamma}{1-\gamma^2} = \oint \rho(\theta,t)\sin(\theta-\Theta-\delta)d\theta,$$
$$\frac{\gamma\dot\Psi}{\sqrt{1-\gamma^2}} = -\oint \rho(\theta,t)\cos(\theta-\Theta-\delta)d\theta,$$
$$\gamma\dot\Theta = \frac{\gamma\dot\Psi}{\sqrt{1-\gamma^2}}.$$

Using (3.4) and (5.5), these equations become

$$\frac{\dot\gamma}{1-\gamma^2} = S(t)\cos\delta + T(t)\sin\delta,$$
$$\frac{\gamma\dot\Psi}{\sqrt{1-\gamma^2}} = \gamma\dot\Theta = T(t)\cos\delta - S(t)\sin\delta, \tag{5.18}$$

where

$$S(t) = \oint \frac{\sqrt{1-\gamma^2}\sin(\psi-\Psi)}{1-\gamma\cos(\psi-\Psi)}\sigma(\psi)d\psi$$
$$T(t) = \oint \frac{\gamma-\cos(\psi-\Psi)}{1-\gamma\cos(\psi-\Psi)}\sigma(\psi)d\psi.$$

This is the infinite-N version of the averaged system. Note that Θ does not appear on the right hand sides, so the essential dynamics is only two-dimensional.

5.2.2. Lyapunov function

It is straightforward to see that when $\sin\delta = 0$,

$$\mathcal{H}(\Psi,\gamma) = \oint \log\left(\frac{1-\gamma\cos(\psi-\Psi)}{\sqrt{1-\gamma^2}}\right)\sigma(\psi)d\psi \tag{5.19}$$

is a conserved quantity for (5.18). For other values of δ, this function is a Lyapunov function since

$$\dot{\mathcal{H}} = R^2\sin\delta, \tag{5.20}$$

where

$$R(t)\exp[i\phi(t)] = \oint \exp(i\theta)\rho(\theta,t)d\theta, \quad R \geq 0;\ \phi \in \mathbb{R} \tag{5.21}$$

denotes the order parameter of the oscillator density.

5.2.3. Phase coherence

By imposing the incoherence constraints (5.11), the set where $\gamma = 0$ becomes synonomous with the incoherent states. Moreover, the Lyapunov function $\mathcal{H}$ vanishes at $\gamma = 0$, and its convexity can be easily shown. As in Section 4.3, $\mathcal{H}$ measures the phase coherence of the oscillators.

The dynamics on the invariant subspaces is governed by $\mathcal{H}$. If $\sin\delta = 0$, $\mathcal{H}$ is conserved, from (5.20). Then $\Psi(t)$ and $\gamma(t)$ are periodic, and the system is completely integrable. If $\sin\delta < 0$, $\mathcal{H}$ decreases monotonically and each trajectory spirals down to the incoherent state $\sigma(\psi)$ that labels the invariant subspace. The manifold of incoherent states is a global attracting set. Finally, if $\sin\delta > 0$, then $\mathcal{H}$ increases and all trajectories (except the incoherent ones) approach the in-phase state. As $t \to \infty$, a δ-function appears in ρ, even when the initial density is smooth.

5.3. Solitons

The previous section contains no surprises; the finite-N results of Section 4 carry over to the continuum limit. Now we turn to new phenomena. We restrict attention to the averaged system with $\sin\delta = 0$, unless stated otherwise. Since this case is completely integrable, we expect to find something analogous to solitary wave solutions [37], traveling at a constant speed without changing shape. We shall see that the averaged system indeed exhibits such solutions. In addition, we study the motion of an individual oscillator when such waves occur, and show that the transformation (5.4) collapses to extremely simple form. Finally, we consider recurrence phenomena for this system.

5.3.1. Traveling waves

Although it is easy to obtain traveling wave solutions starting from the usual assumption $\rho(\theta,t) = \rho(\theta - Ut)$, we take a more indirect approach here to illuminate the geometrical interpretation of the traveling waves.

Recall that the phase space is partitioned into a family of three-dimensional invariant subspaces, parametrized by the incoherent density $\sigma(\psi)$. The dynamics on each of the subspaces is similar; they all have the same Lyapunov function.

Still, one of the subspaces occupies a special position geometrically. It is the subspace corresponding to the uniform distribution $\sigma(\psi) =$ constant. It corresponds to the splay state of the finite-N case, where the oscillators' phases are equally spaced. For $N = 4$, this subspace is the membrane shown in Fig. 12b.

The splay state for $N = 3$ and $N = 4$ lies at the center of the canonical invariant region, as shown in Figs. 10–13. Moreover, it is the center of the incoherent manifold itself (the dashed filament in Figs. 11–13). By analogy, we expect that the uniform distribution state for the continuum limit is located at the center of both the phase space and the incoherent manifold. The subspace parametrized by, and emanating from, this state is expected to be the most symmetric of all the subspaces. In fact, this is the *subspace of all possible traveling wave solutions.*

To see this, we derive the waves directly from the reduced equations (5.18). As noted, the special subspace is parametrized by the uniform density

$$\sigma(\psi) = \frac{1}{2\pi}. \tag{5.22}$$

The integrals in (5.18) are now easy to evaluate:

$$\oint \frac{\sin(\psi - \Psi)}{1 - \gamma\cos(\psi - \Psi)} \frac{1}{2\pi} d\psi = \frac{1}{2\pi} \oint \frac{\sin\xi}{1 - \gamma\cos\xi} d\xi = 0,$$

$$\oint \frac{\gamma - \cos(\psi - \Psi)}{1 - \gamma\cos(\psi - \Psi)} \frac{1}{2\pi} d\psi = \frac{1}{2\pi\gamma} \oint \left(1 - \frac{1 - \gamma^2}{1 - \gamma\cos\xi}\right) d\xi = \frac{1 - \sqrt{1 - \gamma^2}}{\gamma}.$$

Hence (5.18) becomes

$$\dot{\gamma} = \sin\delta \frac{(1 - \gamma^2)(1 - \sqrt{1 - \gamma^2})}{\gamma},$$

$$\gamma\dot{\Theta} = \frac{\gamma\dot{\Psi}}{\sqrt{1 - \gamma^2}} = \cos\delta \frac{1 - \sqrt{1 - \gamma^2}}{\gamma}.$$

It is more convenient to use $\alpha = (1 - \gamma^2)^{-1/2}$. The equations then become

$$\dot{\alpha} = (\alpha - 1)\sin\delta, \quad \frac{\dot{\Theta}}{\alpha} = \dot{\Psi} = \frac{\cos\delta}{\alpha + 1}.$$

The solution can be obtained explicitly. Assume $\Theta(0) = \Psi(0) = 0$ for simplicity. Then the solution is

$$\alpha(t) = 1 + (\alpha_0 - 1)\,e^{t\sin\delta},$$

$$\Theta(t) = \tfrac{1}{2}\cot\delta \left[3t\sin\delta - \log\left(\frac{2 + (\alpha_0 - 1)\,e^{t\sin\delta}}{\alpha_0 + 1}\right)\right],$$

$$\Psi(t) = \tfrac{1}{2}\cot\delta \left[t\sin\delta - \log\left(\frac{2 + (\alpha_0 - 1)\,e^{t\sin\delta}}{\alpha_0 + 1}\right)\right].$$

In particular, when $\sin\delta = 0$ (and we let $\delta = 0$ without loss of generality), this reduces to

$$\alpha(t) = \alpha_0 \quad (\gamma(t) = \gamma_0), \quad \Theta(t) = Ut, \quad \Psi(t) = Vt,$$

where α_0, γ_0, and

$$U = \frac{\alpha}{\alpha + 1} = \frac{1 - \sqrt{1 - \gamma^2}}{\gamma^2}, \quad V = \frac{1}{\alpha + 1} = \frac{\sqrt{1 - \gamma^2} - (1 - \gamma^2)}{\gamma^2}$$

are all constants.

From now on, focus on this integrable case $\sin\delta = 0$. Since α (or γ) is constant, the mapping used in the transformation (5.4) is stationary. Since the preimage $\sigma(\psi)$ is always stationary, the image $\rho(\theta, t)$ also looks stationary in the frame moving with $\Theta(t)$. Moreover, the speed of the frame is the constant $\dot{\Theta} = U$. Hence, this solution represents a traveling wave in the θ-coordinate. Fig. 14 illustrates these relations.

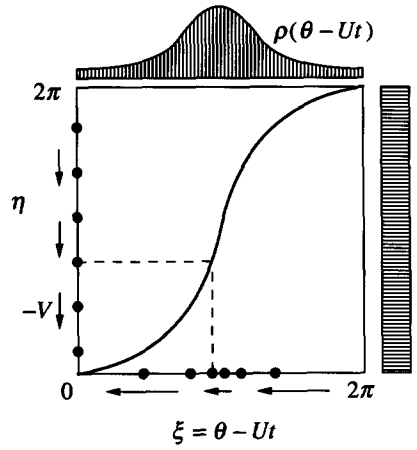

Fig. 14. Change of coordinates for the traveling wave solutions. In this simple case, the mapping curve is fixed since the distortion γ reduces to a constant. The preimage density $\sigma(\psi)$ is uniform. Individual oscillators move at uniform velocity $-V$ with respect to ψ. In the original coordinates, the oscillators move non-uniformly, hesitating near the peak of the density ρ and running rapidly in between.

The shape of the traveling wave follows from (5.16). We obtain

$$\rho(\theta,t) = \sigma\left(\frac{\partial\theta}{\partial\psi}\right)^{-1} = \frac{1}{2\pi}\frac{\sqrt{1-\gamma^2}}{1+\gamma\cos(\theta-\Theta)} = \frac{1}{2\pi}\frac{\sqrt{1-\gamma^2}}{1+\gamma\cos(\theta-Ut)}, \tag{5.23}$$

where we have written simply γ instead of γ_0. This solution is a solitary bump on the circle. It involves one parameter γ. When $\gamma = 0$, the solution reduces to the uniform distribution, i.e., the preimage $\sigma(\psi)$ itself. As γ increases, the height of the bump grows monotonically, and diverges when $\gamma \to 1$, since

$$\rho_{\max} = \max_{\xi}\frac{1}{2\pi}\frac{\sqrt{1-\gamma^2}}{1+\gamma\cos\xi} = \frac{1}{2\pi}\frac{\sqrt{1-\gamma^2}}{1-\gamma} = \frac{1}{2\pi}\sqrt{\frac{1+\gamma}{1-\gamma}}.$$

The wave speed U changes from $1/2$ ($\gamma = 0$ or $\alpha = 1$) to 1 ($\gamma \to 1$ or $\alpha \to \infty$) monotonically – taller waves travel faster.

The velocity field $v(\theta,t)$ is obtained from (5.3) by substituting (5.17) and setting $\delta = 0$:

$$v(\theta,t) = \oint \rho(\theta',t)\cos(\theta'-\theta-\delta)d\theta'\Big|_{\delta=0} = \frac{\sqrt{1-\gamma^2}}{2\pi}\oint\frac{\cos(\theta'-\theta)d\theta'}{1+\gamma\cos(\theta'-Ut)}$$
$$= -A\cos(\theta-Ut),$$

$$A = \frac{1-\sqrt{1-\gamma^2}}{\gamma}.$$

Here v is the speed of individual oscillators in the *stationary* frame. In the frame of the traveling wave, the velocity of an oscillator becomes

$$v(\theta,t) - U = -[U + A\cos\xi], \quad \xi = \theta - Ut.$$

It is easy to show that $0 \le A < U < 1$ for $0 \le \gamma < 1$. Hence the oscillators always move backward relative to the density wave, and their speed is nonuniform; they hesitate near the peak of ρ

($\xi = \pm\pi$) and run rapidly through the trough ($\xi = 0$). In other words, each oscillator lingers near all the others until the time comes for it to "phase slip" abruptly.

5.3.2. Transformation

Now suppose we wish to convert the nonuniform motion of an individual oscillator into *uniform* motion by changing variables from $\xi = \theta - Ut$ (nonuniform) to, say, η (uniform). The standard technique is to use the *time of travel* as the new coordinate. The time required for an oscillator to travel from $\xi = 0$ to ξ is

$$\int_0^{\xi} \frac{d\xi}{\dot{\xi}} = \int_0^{\xi} \frac{d\xi}{-(U + A\cos\xi)} = -\frac{2}{\sqrt{U^2 - A^2}} \arctan\left(\frac{\sqrt{U^2 - A^2}}{U + A} \tan(\tfrac{1}{2}\xi)\right).$$

This must equal to the amount of time for the oscillator to travel from $\eta = 0$ to η at a constant speed W. Hence

$$\frac{\eta}{W} = -\frac{2}{\sqrt{U^2 - A^2}} \arctan\left(\frac{\sqrt{U^2 - A^2}}{U + A} \tan(\tfrac{1}{2}\xi)\right).$$

Also, we require that $\eta = \pm\pi$ when $\xi = \pm\pi$ so that the period agrees in both coordinates. Then the constant W is determined as

$$W = -\sqrt{U^2 - A^2} = -\left[\left(\frac{1}{\gamma^4} - \frac{1}{\gamma^2}\right) \cdot (1 - \sqrt{1 - \gamma^2})^2\right]^{1/2} = -\frac{\sqrt{1 - \gamma^2} - (1 - \gamma^2)}{\gamma^2} = -V.$$

Thus V denotes the converted, uniform speed of the oscillators. The transformation now becomes

$$\eta = 2\arctan\left(\frac{\sqrt{U^2 - A^2}}{U + A} \tan[\tfrac{1}{2}(\theta - Ut)]\right).$$

Next observe that the phase configuration rotates rigidly in the new coordinates, since all the oscillators have the same uniform velocity. Therefore, by going into yet another rotating frame, the oscillators can be made to appear motionless or *frozen*. This is achieved by introducing a new coordinate ψ, where

$$\eta = \psi - Vt.$$

Hence the overall transformation is

$$\tan[\tfrac{1}{2}(\theta - Ut)] = \frac{U + A}{\sqrt{U^2 - A^2}} \tan[\tfrac{1}{2}(\psi - Vt)].$$

Since

$$\frac{U + A}{\sqrt{U^2 - A^2}} = \frac{U + A}{V} = \frac{1 + \gamma}{\sqrt{1 - \gamma^2}} = \sqrt{\frac{1 + \gamma}{1 - \gamma}},$$

we have recovered the transformation (3.2) for this particular case:

$$\tan[\tfrac{1}{2}(\theta - Ut)] = \sqrt{\frac{1 + \gamma}{1 - \gamma}} \tan[\tfrac{1}{2}(\psi - Vt)]. \tag{5.24}$$

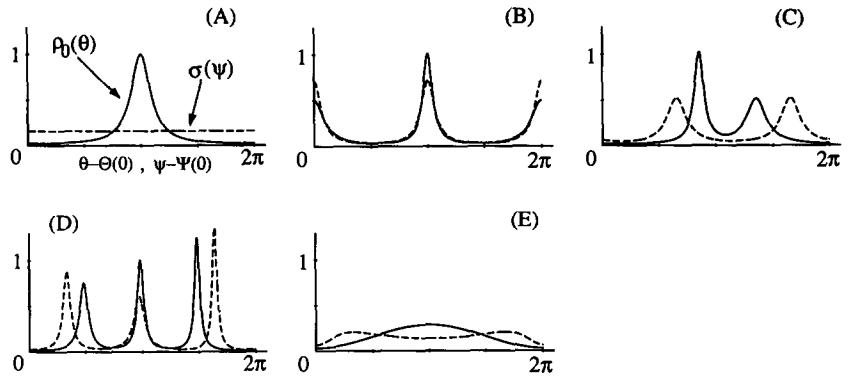

Fig. 15. Five initial densities $\rho_0(\theta)$ (solid curves) and their computed preimages $\sigma(\psi)$ (dashed curves) are shown. The preimages are incoherent, as required by the constraint (5.12). Note that ρ_0 and σ are shown translated by the amounts $\Theta(0)$ and $\Psi(0)$, respectively. Details of the cases (A)–(E) are given in Table 1. (A) 1-soliton; (B) 2-soliton, π apart; (C) 2-soliton, $\pi/2$ apart; (D) 3-soliton; (E) sinusoidal.

Thus, on this most symmetric subspace of solutions, the distortion parameter γ becomes a constant while the two characteristic phases Ψ and Θ are just linear in t.

As mentioned in Section 3.1, the transformation (3.2) between θ and ψ was inspired by these travelling waves. A slight generalization was required to extend to finite N: the three constants U, V, γ in (5.24) had to be replaced by time-dependent functions evolving according to (3.6). But the freezing of the oscillators in the ψ frame carried over perfectly to finite N: as shown earlier, all solutions of (3.1) can be written in the form (3.2), where $\{\psi_j\}$ is *constant* on trajectories.

5.4. *Numerical results*

We now present numerical experiments to illustrate the motion and interaction of solitons. The numerical integrations were done using the reduced system (5.9), expressed in Cartesian-type coordinates as in (3.9)–(3.11), and using (5.11) to convert the initial condition. The validity of the method was confirmed by comparing the results to those obtained from a conventional spectral method applied to the original system (5.2) and (5.3).

5.4.1. *Converted densities*

Fig. 15 shows five initial densities $\rho_0(\theta)$, two of which are to be used in the simulations discussed below. For each $\rho_0(\theta)$, we compute its preimage density $\sigma(\psi)$, as well as the values of (γ, Ψ, Θ), by solving (5.13)–(5.16). Table 1 summarizes the cases.

In case (A), $\rho_0(\theta)$ is the 1-soliton solution (5.23), with parameters $\gamma(0) = \gamma_1$ and $\Theta(0) = \theta_1$. The peak is at $\theta = \theta_1 \pm \pi$. For such a 1-soliton initial condition, it is easy to find the minimum of $U(\Theta, \gamma)$ in (5.14). One can show that $\gamma = \gamma_1$ and $\Theta = \theta_1$ satisfies (5.13). Using these values, Ψ from (5.15) and $\sigma(\psi)$ from (5.16) can be computed. The preimage $\sigma(\psi)$ is a constant function, $\sigma(\psi) = 1/2\pi$. This was to be expected, since the 1-soliton solution $\rho_0(\theta)$ lies on the manifold parametrized by the splay state.

In cases (B) and (C), $\rho_0(\theta)$ is a superposition of two solitons with different amplitudes. (The density $\rho_0(\theta)$ must be divided by 2 to normalize it after superposition.) The phase difference between the two pulses is π for (B) and $\pi/2$ for (C). The amplitude parameters γ_1 and γ_2 for both

Table 1
Five initial densities $\rho_0(\theta)$ and the corresponding initial conditions for the reduced variables, obtained by solving (5.13)–(5.16). The resulting incoherent preimages $\sigma(\psi)$ are shown in Fig. 15. In the table, $\rho_W(\theta;\gamma_j,\theta_j) = (1/2\pi)[(1-\gamma_j^2)^{1/2}/(1+\gamma_j\cos(\theta-\theta_j))]$ denotes the traveling wave solution with an amplitude parameter γ_j and a translational offset θ_j. Angular variables are shown within $[-\pi,\pi]$.

Case	$\rho_0(\theta)$	$\gamma(0)$	$\Psi(0)/\pi$	$\Theta(0)/\pi$
(A)	$\rho_W(\theta\gamma_1,\theta_1)$	0.9505910	0	0.2500000
(B)	$\frac{1}{2}\sum_{j=1}^{2}\rho_W(\theta;\gamma_j,\theta_j)$	0.3333333	0	−0.7500000
(C)	$\frac{1}{2}\sum_{j=1}^{2}\rho_W(\theta;\gamma_j,\theta_j)$	0.7285979	−0.1040134	−0.6048600
(D)	$\frac{1}{3}\sum_{j=1}^{3}\rho_W(\theta;\gamma_j,\theta_j)$	0.4614420	−0.0826765	−0.7316964
(E)	$\frac{1}{2\pi}(1+\frac{4}{5}\sin\theta)$	0.6246950	0	−0.5000000

In this column, the parameter values are:
(A) $\gamma_1 = 0.9505910$, $\theta_1 = \pi/4$,
(B) $\gamma_1 = 0.9874146$, $\theta_1 = -3\pi/4$, $\gamma_2 = 0.9505910$, $\theta_2 = \pi/4$,
(C) $\gamma_1 = 0.9874146$, $\theta_1 = -3\pi/4$, $\gamma_2 = 0.9505910$, $\theta_2 = -\pi/4$,
(D) $\gamma_1 = 0.9900428$, $\theta_1 = 3\pi/4$, $\gamma_2 = 0.9943868$, $\theta_2 = -3\pi/4$, $\gamma_3 = 0.9964039$, $\theta_3 = -\pi/4$.

cases are chosen such that the height of the two peaks are 1 and 1/2. In both cases, the computed preimages $\sigma(\psi)$ consist of two almost symmetric bumps roughly π apart. The calculated $\sigma(\psi)$ satisfied the constraints (5.11) and (5.12) within numerical accuracy.

For these cases, the computed values of $\gamma(0)$ and $\Theta(0)$ (Table 1) are not obvious combinations of the parameters $\gamma_{1,2}$ and $\theta_{1,2}$ (although case (B) seems simple). Rather, they are obtained by minimizing $\mathcal{U}$. This potential function $\mathcal{U}$ itself *is* superposable as seen from (5.14). That is, if two densities $\rho_1(\theta)$ and $\rho_2(\theta)$ correspond to $\mathcal{U}_1$ and $\mathcal{U}_2$, respectively, then the potential corresponding to $\rho_0(\theta) = (\rho_1+\rho_2)/2$ is $\mathcal{U}(\Theta,\gamma) = (\mathcal{U}_1+\mathcal{U}_2)/2$. For the cases (B) and (C), ρ_1 and ρ_2 are two 1-soliton solutions. Then, $\min\mathcal{U}_1$ and $\min\mathcal{U}_2$ are achieved at (θ_1,γ_1) and (θ_2,γ_2), respectively. Unfortunately, (Θ,γ) is not a linear combination of these two, but is obtained in a more elaborate manner through minimization of the superposed potential functions.

The remaining two cases (D) and (E) correspond to 3-soliton or sinusoidal initial densities, respectively. The preimages are found to have somewhat irregular shapes.

5.4.2. *Soliton interactions for an integrable system*

For cases (B) and (C) above, we now consider the evolution of $\rho(\theta,t)$, assuming that the system is governed by the completely integrable averaged system (5.2, 5.3, 5.17) with $\delta = 0$.

Fig. 16 shows the evolution for case (B). In Fig. 16a, we plot $\gamma(t)$, $\Psi(t)$, and $\Theta(t)$ of the reduced equations, over one period of $\Psi(t)$. (The period $T \approx 16.8$.) The other phase variable $\Theta(t)$ also seems to advance by 2π during this period. The distortion parameter $\gamma(t)$ oscillates twice during one period. The periodicity is made clearer in Fig. 16b, which plots the trajectory using (γ,Ψ) as polar coordinates. As expected, the trajectory is a closed loop, corresponding to a contour of the Hamiltonian $\mathcal{H}$ in (5.19). The loop is small, indicating that the initial condition $\rho_0(\theta)$ is fairly close to an incoherent state. Since γ never assumes large values, we expect the image $\rho(\theta,t)$ to be a slight distortion of the preimage $\sigma(\psi)$ for all time.

In Fig. 16c the evolution of $\rho(\theta,t)$ is displayed directly. The spatial coordinate is co-moving with $\Theta(t)$. Therefore, only variations due to γ and Ψ should be visible in the figure, and we should see periodic motion with period T. Indeed, such recurrence is observed, the first and the

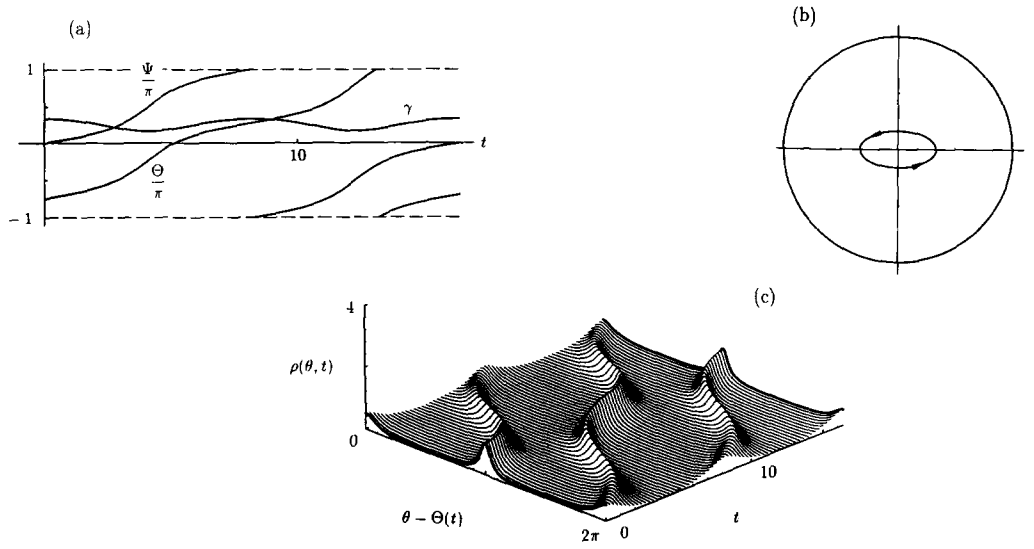

Fig. 16. Evolution of the 2-soliton case (B) for the integrable averaged system. One period of the (γ, Ψ)-dynamics ($T \approx 16.8$) is plotted here.
(a) Solution of the reduced equations. (b) In the polar diagram of γ and Ψ, the projected trajectory is a small loop. (c) The density $\rho(\theta, t)$, plotted in a frame co-moving with $\Theta(t)$. Two peaks persist for all time.

last waveforms being identical. Because of the small distortion from the preimage, the two pulses are distinguishable for all time, although an exchange of their identities can be seen.

Fig. 17 plots the evolution for case (C) in a similar manner. Again, one period in $\Psi(t)$ is computed ($T \approx 19.2$), but now $\Theta(t)$ advances more than 2π, probably because of the asymmetric shape of ρ_0 (Fig. 17a). The trajectory in Fig. 17b is still periodic, but the loop is much larger than in the previous case. Since γ becomes close to 1, we see a rather different picture of $\rho(\theta, t)$. As shown in Fig. 17c, one of the two pulses disappears and is completely absorbed by the other, then emerges from the other side.

In Figs. 16 and 17, one might be misled into thinking that the fundamental period of $\rho(\theta, t)$ is $T/2$, not T. This is because the preimage $\sigma(\psi)$ is almost symmetric, and the trajectory in (γ, Ψ) polar coordinates is almost an ellipse. The true periodicity is clearer for trajectories starting from less symmetric initial densities like (D) and (E) (results not shown).

5.4.3. *Chaotic waves for a non-averaged system*

At the end of Section 3, we pointed out that KAM-like chaos can occur in the resistively loaded array. We now present numerical results illustrating similar chaos for the continuum limit. The point is not that the chaos is particularly dramatic (it isn't), but rather that the system provides a simple, explicit example of an infinite-dimensional system whose dynamical complexity is rigorously bounded (the system's reducibility implies that the chaos is at most three-dimensional).

Consider the Josephson junction array equations (3.16) for the case of a pure resistive load. In the limit $N \to \infty$, the equations give the velocity field

$$v(\theta, t) = 1 + a \sin\theta + \varepsilon \oint \rho(\varphi, t) \sin\varphi d\varphi, \tag{5.25}$$

which should be used in the continuity equation (5.2). The system is reducible, since the velocity

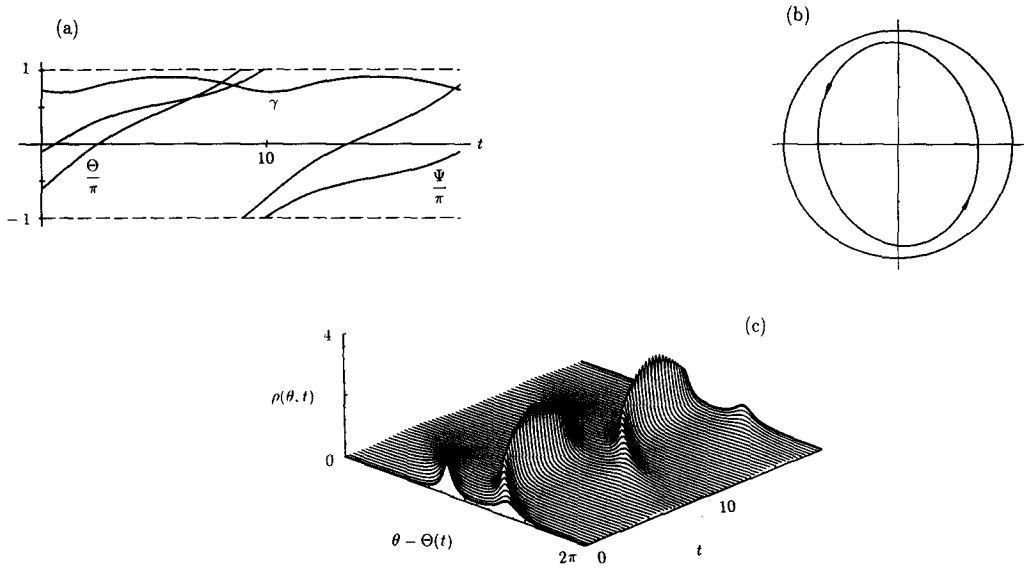

Fig. 17. Evolution of the 2-soliton case (C) for the integrable averaged system, plotted as in Fig. 16. Here $T \approx 19.2$. (a) Solution of the reduced equations. (b) In the polar diagram of γ and Ψ, the projected trajectory is a large loop. (c) The density $\rho(\theta,t)$. One pulse is absorbed by the other to form a sharp spike, but re-emerges.

takes the form (5.3) with

$$f = 1 + \varepsilon \oint \rho(\varphi,t)\sin\varphi d\varphi\,, \quad g = 0\,, \quad h = a\,. \tag{5.26}$$

We numerically integrated (5.9), for $a = 2$ and $\varepsilon = -2$. Instead of specifying the initial density $\rho_0(\theta)$, the preimage density $\sigma(\psi)$, and the initial values of (x,y,Φ) were input directly. Fig. 18 shows a chaotic case corresponding to

$$\sigma(\psi) = \frac{1}{2\pi}[1 - \tfrac{3}{4}\sin(3\psi)]\,, \quad x(0) = 0\,, \quad y(0) = -0.09\,, \quad \Phi(0) = 0\,.$$

The chaos is not obvious in Fig. 18a; one would need to integrate much longer to see it, but then the graph would become cluttered with uninteresting details. It is more revealing to plot a Poincaré-section. Fig. 18b shows a section taken at $\Phi = \Phi(0) \pmod{2\pi}$. The coordinates are x and y as in Fig. 4. The section consists of 1,000 returns, computed by integration up to $t = 6283$. The trajectory seems to be part of a "chaotic sea"; it does not explore the entire region, but appears to be confined between invariant tori. Fig. 18c shows $\rho(\theta,t)$ over the same short time interval used in Fig. 18a. For clarity, the density is plotted in a frame moving with $\Theta(t)$. Small initial fluctuations grow and form two sharp spikes, then decay. Although this plot suggests that the situation is nearly recurrent, Fig. 18b strongly suggests that the dynamics is chaotic on a longer time scale.

6. Open questions

We conclude with some suggestions for future research.

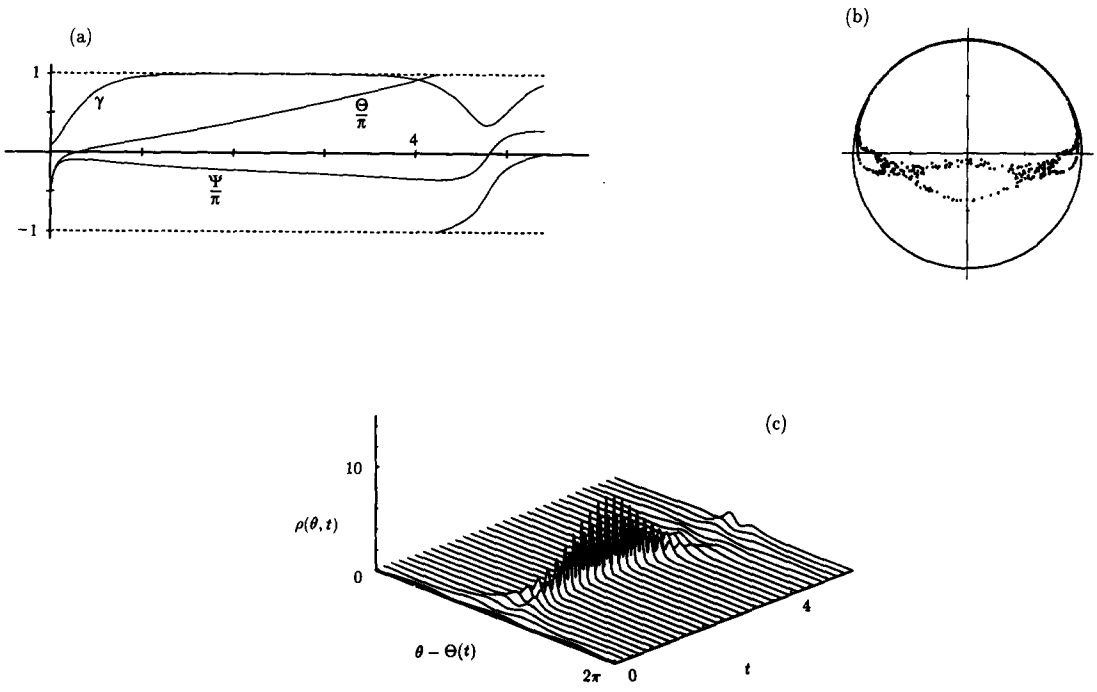

Fig. 18. Chaotic evolution of a wave in a reducible but non-integrable system (the resistively loaded Josephson array in the continuum limit). The parameters are $a = 2$ and $\varepsilon = -2$. (a) Solution of the reduced equations, for $t \leq 5.4$. (b) Chaos is visible in the Poincaré-section at $\Phi = \Phi(0) \pmod{2\pi}$, obtained by computing up to $t = 6283$. (c) Evolution of density $\rho(\theta, t)$, for $t \leq 5.4$.

(1) Our analysis of Josephson arrays is restricted to the limit of overdamped junctions ($\beta = 0$). But there is numerical evidence [3] that even if $\beta > 0$, certain arrays still have enormously degenerate phase space structure. Does a high-dimensional manifold of incoherent states exist for these systems as well?

(2) For the overdamped systems studied here, we have shown (Section 3) that the dynamics can be reduced to a much smaller set of differential equations. Specifically, the dynamics of the N-dimensional system (3.1) is captured completely by the 3-dimensional system (3.6). Unfortunately, the reduced system appears intractable. Can one make progress on its analysis?

(3) Can one find a connection between the partially integrable systems studied here, and more familiar integrable many-body systems like the Toda lattice [37]?

(4) In any case, is there a more algebraic interpretation of the constants of motion? Goebel has recently obtained some elegant results in this direction [38].

Acknowledgments

Jim Swift provided many helpful suggestions throughout this project. Thanks to Jim Swift and Kurt Wiesenfeld for their comments on a draft of this paper. Research supported by a National Science Foundation Presidential Young Investigator award to S.H.S., and NSF Grant DMS-9111497.

Appendix A. Reduction of continuum limit systems

This appendix provides details of the reduction discussed in Section 5.1. In particular, we derive the three equations in (5.9), starting from (5.2) and (5.3).

We first express $\partial(\rho v)/\partial\theta$ in (5.2) in terms of the new coordinates. From (5.5) and (5.8),

$$\rho(\theta,t) = \sigma(\psi)\frac{\partial\psi}{\partial\theta} = \sigma(\psi)\frac{1-\gamma\cos(\psi-\Psi)}{\sqrt{1-\gamma^2}}. \tag{A.1}$$

Using (3.4), v in (5.3) can be rewritten as

$$\begin{aligned}(1-\gamma\cos(\psi-\Psi))v = {} & f(1-\gamma\cos(\psi-\Psi)) \\ & + g\left[-\gamma\cos\Theta + \cos\Theta\cos(\psi-\Psi) - \sqrt{1-\gamma^2}\sin\Theta\sin(\psi-\Psi)\right] \\ & + h\left[-\gamma\sin\Theta + \sin\Theta\cos(\psi-\Psi) + \sqrt{1-\gamma^2}\cos\Theta\sin(\psi-\Psi)\right].\end{aligned}$$

Thus,

$$\begin{aligned}\frac{\partial}{\partial\theta}(\rho v) &= \frac{\partial\psi}{\partial\theta}\frac{\partial}{\partial\psi}(\rho v) \\ &= \frac{1-\gamma\cos(\psi-\Psi)}{\sqrt{1-\gamma^2}}\frac{1}{\sqrt{1-\gamma^2}}\frac{\partial}{\partial\psi}[\sigma(\psi)(1-\gamma\cos(\psi-\Psi))v] \\ &= \frac{1-\gamma\cos(\psi-\Psi)}{1-\gamma^2}\{\sigma'(\psi)[f(1-\gamma\cos(\psi-\Psi)) \\ &\quad + g(-\gamma\cos\Theta + \cos\Theta\cos(\psi-\Psi) - \sqrt{1-\gamma^2}\sin\Theta\sin(\psi-\Psi)) \\ &\quad + h(-\gamma\sin\Theta + \sin\Theta\cos(\psi-\Psi) + \sqrt{1-\gamma^2}\cos\Theta\sin(\psi-\Psi))] \\ &\quad + \sigma(\psi)[\gamma f\sin(\psi-\Psi) + g(-\cos\Theta\sin(\psi-\Psi) - \sqrt{1-\gamma^2}\sin\Theta\cos(\psi-\Psi)) \\ &\quad + h(-\sin\Theta\sin(\psi-\Psi) + \sqrt{1-\gamma^2}\cos\Theta\cos(\psi-\Psi))]\}.\end{aligned} \tag{A.2}$$

Next, compute $\partial\rho/\partial t$ by

$$\frac{\partial\rho}{\partial t} = \frac{\partial\rho}{\partial\tau} + \frac{\partial\psi}{\partial t}\frac{\partial\rho}{\partial\psi}, \tag{A.3}$$

where τ is the "new" time coordinate and $\tau = t$. From (A.1), we find

$$\begin{aligned}\frac{\partial\rho}{\partial\tau} &= \sigma(\psi)\frac{\partial}{\partial\tau}\left(\frac{1-\gamma(\tau)\cos[\psi-\Psi(\tau)]}{\sqrt{1-\gamma(\tau)^2}}\right) \\ &= \frac{\sigma(\psi)}{(1-\gamma^2)^{3/2}}\{(1-\gamma^2)[-\dot\gamma\cos(\psi-\Psi) - \gamma\dot\Psi\sin(\psi-\Psi)] + \gamma\dot\gamma[1-\gamma\cos(\psi-\Psi)]\} \\ &= \frac{\sigma(\psi)}{(1-\gamma^2)^{3/2}}[\dot\gamma(\gamma-\cos(\psi-\Psi)) - \gamma\dot\Psi(1-\gamma^2)\sin(\psi-\Psi)]\end{aligned} \tag{A.4}$$

and

$$\frac{\partial\rho}{\partial\psi} = \frac{\partial}{\partial\psi}\left(\sigma(\psi)\frac{1-\gamma(\tau)\cos(\psi-\Psi(\tau))}{\sqrt{1-\gamma(\tau)^2}}\right)$$

$$= \frac{\sigma'(\psi)}{\sqrt{1-\gamma^2}}(1-\gamma\cos(\psi-\Psi)) + \frac{\sigma(\psi)}{\sqrt{1-\gamma^2}}\gamma\sin(\psi-\Psi). \tag{A.5}$$

From this point on, only algebraic manipulations follow. For brevity, let $c = \cos(\psi-\Psi)$ and $s = \sin(\psi-\Psi)$. Substituting (5.7), (A.4), and (A.5) into (A.3), we obtain

$$\begin{aligned}(1-\gamma^2)^{3/2}\frac{\partial\rho}{\partial t} &= \sigma[\dot\gamma(\gamma-c) - \gamma\dot\Psi(1-\gamma^2)s] \\ &\quad + [\dot\Psi(1-\gamma^2) - \dot\gamma s - \dot\Theta\sqrt{1-\gamma^2}(1-\gamma c)][\sigma'(1-\gamma c) + \sigma\gamma s] \\ &= \sigma[\dot\gamma(\gamma-c-\gamma s^2) - \gamma s\sqrt{1-\gamma^2}(1-\gamma c)\dot\Theta] \\ &\quad + \sigma'(1-\gamma c)[\dot\Psi(1-\gamma^2) - \dot\gamma s - \dot\Theta\sqrt{1-\gamma^2}(1-\gamma c)].\end{aligned}$$

Since

$$\gamma - c - \gamma s^2 = \gamma - c - \gamma(1-c^2) = -c(1-\gamma c),$$

the final expression becomes

$$\frac{(1-\gamma^2)^{3/2}}{1-\gamma c}\frac{\partial\rho}{\partial t} = \sigma[-\dot\gamma c - \gamma s\sqrt{1-\gamma^2}\dot\Theta] + \sigma'[\dot\Psi(1-\gamma^2) - \dot\gamma s - \dot\Theta\sqrt{1-\gamma^2}(1-\gamma c)]. \tag{A.6}$$

We can now express the continuity equation (5.2) in the new coordinate system. Rewrite (A.2) as

$$\begin{aligned}\frac{(1-\gamma^2)^{3/2}}{1-\gamma c}\frac{\partial(\rho v)}{\partial\theta} &= \sigma'\sqrt{1-\gamma^2}[f(1-\gamma c) + g(-\gamma\cos\Theta + c\cos\Theta - s\sqrt{1-\gamma^2}\sin\Theta) \\ &\quad + h(-\gamma\sin\Theta + c\sin\Theta + s\sqrt{1-\gamma^2}\cos\Theta)] \\ &\quad + \sigma\sqrt{1-\gamma^2}[\gamma f s + g(-s\cos\Theta - c\sqrt{1-\gamma^2}\sin\Theta) \\ &\quad + h(-s\sin\Theta + c\sqrt{1-\gamma^2}\cos\Theta)].\end{aligned} \tag{A.7}$$

Substitution of (A.6) and (A.7) into (5.2) yields

$$\begin{aligned}0 &= \frac{(1-\gamma^2)^{3/2}}{1-\gamma c}\left(\frac{\partial\rho}{\partial t} + \frac{\partial}{\partial\theta}(\rho v)\right) \\ &= \sigma\{c[-\dot\gamma - g(1-\gamma^2)\sin\Theta + h(1-\gamma^2)\cos\Theta] \\ &\quad + s\sqrt{1-\gamma^2}(-\gamma\dot\Theta + \gamma f - g\cos\Theta - h\sin\Theta)\} \\ &\quad + \sigma'\{\sqrt{1-\gamma^2}(\dot\Psi\sqrt{1-\gamma^2} - \dot\Theta + f - \gamma g\cos\Theta - \gamma h\sin\Theta) \\ &\quad + c\sqrt{1-\gamma^2}(\gamma\dot\Theta - \gamma f + g\cos\Theta + h\sin\Theta) \\ &\quad + s[-\dot\gamma - g(1-\gamma^2)\sin\Theta + h(1-\gamma^2)\cos\Theta]\}.\end{aligned}$$

This equation is satisfied for all t regardless of $\sigma(\psi)$, $c = \cos(\psi-\Psi)$, and $s = \sin(\psi-\Psi)$ if

$$\begin{aligned}&-\dot\gamma - g(1-\gamma^2)\sin\Theta + h(1-\gamma^2)\cos\Theta = 0, \\ &-\gamma\dot\Theta + \gamma f - g\cos\Theta - h\sin\Theta = 0, \\ &\dot\Psi\sqrt{1-\gamma^2} - \dot\Theta + f - \gamma g\cos\Theta - \gamma f\sin\Theta = 0.\end{aligned}$$

These are equivalent to the three equations in (5.9).

Appendix B. Symmetric constants of motion

B.1. Introduction

This appendix is concerned exclusively with the finite-N averaged system (4.1), or equivalently (4.2), with $\sin\delta = 0$. We prove that this system is completely integrable, using a more algebraic approach than in Section 4.

Recall that in the first proof, the integrability followed from the existence of $N-2$ independent constants of motion, namely $\{\psi_j\}$ (only $(N-3)$ of which are independent) and $\mathcal{H}$. The system was thus found to be reducible to a one-degree-of-freedom Hamiltonian system. This approach is similar in spirit to the inverse scattering technique [27,37] for integrable Hamiltonian systems. Our preimage $\{\psi_j\}$ is reminiscent of the time-independent eigenvalues in Lax's formalism, and the functions (γ, Ψ, Θ) are analogous to the time-dependent part of the scattering data. (We stress, however, that this analogy is very loose. In particular, (4.1) does *not* arise from the conservative limit of the Josephson junction equations, but rather the extremely overdamped limit. Moreover, our governing equations are not formulated explicitly in terms of a Hamiltonian.)

For the case of the Toda lattice [37], Flaschka found constants of motion of this scattering type [39]. A different set of constants, however, was found independently by Hénon [40] by direct algebraic methods. These constants have the virtue of being symmetric in their indices, but they are harder to obtain systematically. The two sets of constants of motion are equivalent to each other [37,39].

We show below that $N-2$ constants of motion of the Hénon type, i.e. symmetric ones, can be found for (4.2), and we discuss their relation to the Flaschka type constants of motion, $\{\psi_j\}$ and $\mathcal{H}$. In Section B.2, one of the constants is written down and its invaraiance is checked explicitly. Then in Section B.3 we use the permutation symmetry of the system to generate many additional constants, $N-2$ of which are proven to be functionally independent. Sections B.4 and B.5 contain several notes on the constants of motion, including their relationship to the constants from Section 4.

We would like to acknowledge the contributions of two other workers, and to thank them for generously sharing their unpublished results. Jim Swift [41] discovered the symmetric constants for the averaged system for $N = 3$ and 4, and conjectured their form for arbitrary N. Charles Goebel [38] found a way to simplify the calculations in this appendix, using Möbius transformations. He also independently realized that systems of the form (3.1) have $N-3$ constants of motion.

B.2. Invariance

For convenience, we define the following shorthand notations:

$$C_{ij} \doteq \cos[\tfrac{1}{2}(\theta_i - \theta_j)], \quad S_{ij} \doteq \sin[\tfrac{1}{2}(\theta_i - \theta_j)], \quad \mathrm{ct}_{ij} \doteq \cot[\tfrac{1}{2}(\theta_i - \theta_j)],$$
$$C_{ii|jk} \doteq \cos[\theta_i - \tfrac{1}{2}(\theta_j + \theta_k)], \quad S_{ii|jk} \doteq \sin[\theta_i - \tfrac{1}{2}(\theta_j + \theta_k)],$$
$$\boldsymbol{C}_{ij} \doteq \cos(\theta_i - \theta_j), \quad \boldsymbol{S}_{ij} \doteq \sin(\theta_i - \theta_j),$$
$$\langle p_1, p_2, p_3, \cdots, p_{N-1}, p_N \rangle \doteq S_{p_1 p_2} S_{p_2 p_3} \cdots S_{p_{N-1} p_N} S_{p_N p_1}.$$

We will often use trigonometric conversion formulas between sums and products, e.g.,

$$C_{31} - C_{32} = \cos(\theta_3 - \theta_1) - \cos(\theta_3 - \theta_2)$$
$$= 2\sin[\tfrac{1}{2}(\theta_1 - \theta_2)]\sin[\theta_3 - \tfrac{1}{2}(\theta_1 + \theta_2)] = 2S_{12}S_{33|12}. \tag{B.1}$$

For the system (4.2) Swift has shown [41] several constants of motion when $N = 3$ or 4:

- for $N = 3$, $I = S_{12}S_{23}S_{31}$ is conserved, and
- for $N = 4$, $J_1 = S_{12}S_{34}$, $J_2 = S_{13}S_{24}$, $J_3 = S_{14}S_{23}$ are all conserved, hence $I = -J_1J_3 = S_{12}S_{23}S_{34}S_{41}$ is also conserved.

Motivated by these results, one expects that

$$I = \langle 1, 2, 3, \cdots, N-1, N\rangle = S_{12}S_{23}\cdots S_{N-1,N}S_{N1} \tag{B.2}$$

is a constant of motion of the system (4.2). Such a conjecture can be proved as follows. Since any θ_i is involved in exactly two of the sine terms in (B.2),

$$\frac{\partial I}{\partial \theta_i} = \tfrac{1}{2}S_{12}S_{23}\cdots S_{i-2,i-1}S_{i-1,i}C_{i,i+1}S_{i+1,i+2}\cdots S_{N-1,N}S_{N1}$$
$$-\tfrac{1}{2}S_{12}S_{23}\cdots S_{i-2,i-1}C_{i-1,i}S_{i,i+1}S_{i+1,i+2}\cdots S_{N-1,N}S_{N1},$$

where the indices are reduced modulo N. A simpler expression is obtained when this is divided by I:

$$\frac{2}{I}\frac{\partial I}{\partial \theta_i} = \mathrm{ct}_{i,i+1} - \mathrm{ct}_{i-1,i}. \tag{B.3}$$

Thus the change of I along a trajectory of (4.2) is

$$\frac{2}{I}\dot{I} = \sum_{i=1}^{N}\frac{2}{I}\frac{\partial I}{\partial \theta_i}\dot{\theta}_i = \sum_{i=1}^{N}(\mathrm{ct}_{i,i+1} - \mathrm{ct}_{i-1,i})\dot{\theta}_i = \sum_{i=1}^{N}\mathrm{ct}_{i,i+1}(\dot{\theta}_i - \dot{\theta}_{i+1}). \tag{B.4}$$

From (4.2),

$$N(\dot{\theta}_1 - \dot{\theta}_2) = (C_{11} + C_{21} + C_{31} + \cdots + C_{N1}) - (C_{12} + C_{22} + C_{32} + \cdots + C_{N2}).$$

C_{11} and C_{22}, C_{21} and C_{12} cancel. Then from (B.1) and analogous identities, we obtain

$$N(\dot{\theta}_1 - \dot{\theta}_2) = (C_{31} - C_{32}) + (C_{41} - C_{42}) + \cdots + (C_{N1} - C_{N2})$$
$$= 2S_{12}S_{33|12} + 2S_{12}S_{44|12} + \cdots + 2S_{12}S_{NN|12}$$
$$= 2S_{12}\left[S_{33|12} + S_{44|12} + \cdots + S_{NN|12}\right].$$

Hence, using a formula similar to (B.1),

$$N\,\mathrm{ct}_{12}\left(\dot{\theta}_1 - \dot{\theta}_2\right) = 2C_{12}\left[S_{33|12} + S_{44|12} + \cdots + S_{NN|12}\right]$$
$$= (S_{31} + S_{32}) + (S_{41} + S_{42}) + \cdots + (S_{N1} + S_{N2}).$$

Each product of a cosine and a sine term was converted back to sums of sine terms.

Similar expressions are obtained for the other indices cyclically. Substitute these expressions into (B.4):

$$\begin{aligned}\frac{2N}{I}\dot{I} = {} & (S_{31} + S_{32}) + (S_{41} + S_{42}) + \cdots + (S_{N-1,1} + S_{N-1,2}) + (S_{N1} + S_{N2}) \\ & + (S_{42} + S_{43}) + (S_{52} + S_{53}) + \cdots + (S_{N,2} + S_{N,3}) + (S_{12} + S_{13}) \\ & + (S_{53} + S_{54}) + (S_{63} + S_{64}) + \cdots + (S_{13} + S_{14}) + (S_{23} + S_{24}) \\ & + \cdots \\ & + (S_{2N} + S_{21}) + (S_{3N} + S_{31}) + \cdots + (S_{N-2,N} + S_{N-2,1}) + (S_{N-1,N} + S_{N-1,1}) .\end{aligned}$$

Disregarding the parentheses, we see that the first term of each row cancels with the last term of the next row. The second term of each row cancels with the second to the last term of two rows below. Similarly, all the terms cancel in pairs and disappear. As a result,

$$\dot{I} = 0 . \tag{B.5}$$

Therefore, I is a constant of motion of (4.2).

To get some intuition about what I measures, observe that I vanishes when $\theta_j = \theta_{j+1}$ for any j from 1 to N. Geometrically,this condition defines the boundary of the canonical invariant region (Section 4.4). On the other hand, I is maximized at the center of this region, corresponding to the splay state. Therefore, I is essentially a measure of the distance from the boundary of the canonical invariant region.

B.3. Independence

Since the system (4.2) is invariant with respect to exchange of two indices, $\theta_i \leftrightarrow \theta_j$, it follows that any quantity of the form

$$I = \langle p_1, p_2, \ldots, p_{N-1}, p_N \rangle = S_{p_1 p_2} S_{p_2 p_3} \cdots S_{p_{N-1} p_N} S_{p_N p_1} \tag{B.6}$$

is a constant of motion as long as $(p_1, \cdots, p_N)$ is a permutation of $(1, \cdots, N)$. By taking all possible permutations, we can generate many constants of motion. Of course, some of the constants of motion are identical (apart from sign) because of the symmetries:

$$\begin{aligned}\langle p_1, p_2, \ldots, p_{N-1}, p_N \rangle &= \langle p_2, p_3, \ldots, p_N, p_1 \rangle \qquad \text{(rotation)}, \\ &= \pm \langle p_N, p_{N-1}, \ldots, p_2, p_1 \rangle \qquad \text{(inversion)}.\end{aligned}$$

However, there still remain $(N-1)!/2$ constants of motion after these symmetries are considered. We show below that a sufficient number of constants of motion for integrability are included in this set.

How many independent constants of motion are required for integrability? Since (4.2) is posed in non-Hamiltonian form, $(N-1)$ constants of motion are necessary, in principle. Actually, we only need $N-2$ constants, because of the rotation invariance of the averaged system; the right hand side of (4.2) depends only on phase differences of oscillators. After a linear change of variables into the mean phase and $(N-1)$ phase differences, we see that the mean phase is decoupled, and is just driven passively by the dynamics of the phase differences. Notice that the constant of motion in (B.6) is also expressed solely in terms of phase differences. In the phase space the surface $I = \text{const.}$ is a cylinder extending in the mean phase direction.

For $N = 3$, we have $(3-1)!/2 = 1$ constants of motion, i.e.

$$I = \langle 1,2,3\rangle = S_{12}S_{23}S_{31} \ .$$

This particular case, therefore, is already completely integrable.

For $N \geq 4$, we have more constants of motion than required. Obviously, there are relationships among them. We now provide a proof that there are $N-2$ *independent* constants of motion out of the set. (Functional relationships among the dependent constants of motion for $N = 4$ and 5 can be found explicitly, as shown in Section B.4.)

Theorem. Consider the following set of $(N-1)$ constants of motion, obtained by cyclically permuting the indices 2 to N:

$$\begin{aligned} I_1 &= \langle 1,2,3,4,\ldots,N-2,N-1,N\rangle, \\ I_2 &= \langle 1,3,4,5,\ldots,N-1,N,2\rangle, \\ I_3 &= \langle 1,4,5,6,\ldots,N,2,3\rangle, \\ &\vdots \\ I_{N-1} &= \langle 1,N,2,3,\ldots,N-3,N-2,N-1\rangle. \end{aligned} \tag{B.7}$$

Then any $N-2$ of these constants are independent.

Proof. We construct the Jacobian matrix and then compute its rank by applying row and column operations. Our goal is to show that the matrix has an $(N-2)\times(N-2)$ minor with non-zero determinant.

Consider the $(N-1)\times(N-1)$ matrix whose (i,j) element is given by $\partial I_i/\partial\theta_j$, $1 \leq i \leq N-1, 2 \leq j \leq N$, chosen to preserve the rotational symmetry of the indices. The elements are simplified by multiplying the ith row by a factor $2/I_i$ to produce similar expressions to (B.3). As a result of this operation, we obtain the matrix

$$\begin{pmatrix} \mathrm{ct}_{23}+\mathrm{ct}_{21} & \mathrm{ct}_{34}+\mathrm{ct}_{32} & \mathrm{ct}_{45}+\mathrm{ct}_{43} & \cdots & \mathrm{ct}_{N-1,N}+\mathrm{ct}_{N-1,N-2} & \mathrm{ct}_{N1}+\mathrm{ct}_{N,N-1} \\ \mathrm{ct}_{21}+\mathrm{ct}_{2N} & \mathrm{ct}_{34}+\mathrm{ct}_{31} & \mathrm{ct}_{45}+\mathrm{ct}_{43} & \cdots & \mathrm{ct}_{N-1,N}+\mathrm{ct}_{N-1,N-2} & \mathrm{ct}_{N2}+\mathrm{ct}_{N,N-1} \\ \mathrm{ct}_{23}+\mathrm{ct}_{2N} & \mathrm{ct}_{31}+\mathrm{ct}_{32} & \mathrm{ct}_{45}+\mathrm{ct}_{41} & \cdots & \mathrm{ct}_{N-1,N}+\mathrm{ct}_{N-1,N-2} & \mathrm{ct}_{N2}+\mathrm{ct}_{N,N-1} \\ \vdots & \vdots & \vdots & \ddots & \vdots & \vdots \\ \mathrm{ct}_{23}+\mathrm{ct}_{2N} & \mathrm{ct}_{34}+\mathrm{ct}_{32} & \mathrm{ct}_{45}+\mathrm{ct}_{43} & \cdots & \mathrm{ct}_{N-1,N}+\mathrm{ct}_{N-1,1} & \mathrm{ct}_{N2}+\mathrm{ct}_{N,N-1} \\ \mathrm{ct}_{23}+\mathrm{ct}_{2N} & \mathrm{ct}_{34}+\mathrm{ct}_{32} & \mathrm{ct}_{45}+\mathrm{ct}_{43} & \cdots & \mathrm{ct}_{N-1,1}+\mathrm{ct}_{N-1,N-2} & \mathrm{ct}_{N2}+\mathrm{ct}_{N1} \end{pmatrix}.$$

The first column, for example, only involves $\mathrm{ct}_{21}, \mathrm{ct}_{23}$ and ct_{2N} since the index 2 in (B.7) is always next to one of the indices 1, 3, or N. Only two entries in this first column involve ct_{21}. All the other entries in this column equal $\mathrm{ct}_{23}+\mathrm{ct}_{2N}$. For the other columns, a similar pattern is observed. Thus, the matrix can be reduced subtracting consecutive rows. For the rows $(N-1),\ldots,2$, subtract each row from the one above. The first row is left unchanged. Then, the matrix becomes

$$\begin{pmatrix} \mathrm{ct}_{23}+\mathrm{ct}_{21} & \mathrm{ct}_{34}+\mathrm{ct}_{32} & \mathrm{ct}_{45}+\mathrm{ct}_{43} & \cdots & \mathrm{ct}_{N-1,N}+\mathrm{ct}_{N-1,N-2} & \mathrm{ct}_{N1}+\mathrm{ct}_{N,N-1} \\ \mathrm{ct}_{2N}-\mathrm{ct}_{23} & \mathrm{ct}_{31}-\mathrm{ct}_{32} & 0 & \cdots & 0 & \mathrm{ct}_{N2}-\mathrm{ct}_{N1} \\ \mathrm{ct}_{23}-\mathrm{ct}_{21} & \mathrm{ct}_{32}-\mathrm{ct}_{34} & \mathrm{ct}_{41}-\mathrm{ct}_{43} & \cdots & 0 & 0 \\ 0 & \mathrm{ct}_{34}-\mathrm{ct}_{31} & \mathrm{ct}_{43}-\mathrm{ct}_{45} & \cdots & 0 & 0 \\ 0 & 0 & \mathrm{ct}_{45}-\mathrm{ct}_{41} & \cdots & 0 & 0 \\ \vdots & \vdots & \vdots & \ddots & \vdots & \vdots \\ 0 & 0 & 0 & \cdots & \mathrm{ct}_{N-1,1}-\mathrm{ct}_{N-1,N-2} & 0 \\ 0 & 0 & 0 & \cdots & \mathrm{ct}_{N-1,N-2}-\mathrm{ct}_{N-1,N} & \mathrm{ct}_{N1}-\mathrm{ct}_{N,N-1} \end{pmatrix}.$$

This matrix can be transformed into upper triangular form [42]. The result is that the diagonal elements of the matrix may be obtained recursively as:

$$\begin{aligned} D_1 &= S_{N2}S_{22|31}, \\ D_2 &= S_{N3}S_{31}S_{33|42} + S_{43}D_1, \\ D_3 &= S_{N4}S_{32}S_{41}S_{44|53} + S_{54}D_2, \\ D_4 &= S_{N5}S_{43}S_{32}S_{51}S_{55|64} + S_{65}D_3, \\ &\vdots \\ D_{N-4} &= S_{N,N-3}S_{N-4,N-5}\cdots S_{32}S_{N-3,1}S_{N-3,N-3|N-2,N-4} + S_{N-2,N-3}D_{N-5}, \\ D_{N-3} &= S_{N,N-2}S_{N-3,N-4}\cdots S_{32}S_{N-2,1}S_{N-2,N-2|N-1,N-3} + S_{N-1,N-2}D_{N-4}, \\ D_{N-2} &= S_{N,N-1}S_{N-2,N-3}\cdots S_{32}S_{N-1,1}S_{N-1,N-1|N,N-2} + S_{N,N-1}D_{N-3}, \\ D_{N-1} &= 0. \end{aligned} \tag{B.8}$$

The rank of the Jacobian matrix is given by the number of non-zero diagonal elements. If there were fewer than $N-2$ independent constants of motion in (B.7), then some of $D_1,\ldots,D_{N-2}$ would have to vanish identically in some open set in the N-dimensional phase space. We show below that this cannot happen. Note that none of S_{ij} terms vanish because of the assumption that $\theta_i \neq \theta_j (i \neq j, \mod 2\pi)$.

First, D_1 vanishes only on $\theta_2 - (\theta_3+\theta_1)/2 = m\pi$, which are $(N-1)$-dimensional planes. Thus, D_1 cannot be identically zero in any open ball in the phase space.

Next, consider D_2 as a function of θ_4 by fixing the phases of the other oscillators. Then, from (B.8), D_2 becomes a linear combination of harmonics: $\sin[\frac{1}{2}\theta_4 - (\theta_3 - \frac{1}{2}\theta_2)]$ and $\sin(\frac{1}{2}\theta_4 - \frac{1}{2}\theta_3)$. Since $\theta_2 \neq \theta_3 + 2m\pi$, it follows that $\theta_3 - \frac{1}{2}\theta_2 \neq \frac{1}{2}\theta_3 + m\pi$. Hence, the two harmonics are out of phase, and their superposition vanishes only at isolated values of θ_4. Therefore D_2 cannot vanish identically in any open ball, either.

Considering D_3 as a function of θ_5, a similar argument applies. We can continue this approach up to D_{N-3}.

Finally, D_{N-2} can be divided by a common factor $S_{N,N-1}$. Then, consider the result as a function of θ_{N-1}. $D_{N-2}/S_{N,N-1}$ becomes a superposition of $\sin(\frac{1}{2}\theta_{N-1} - \frac{1}{2}\theta_1)\sin[\theta_{N-1} - \frac{1}{2}(\theta_N + \theta_{N-2})]$, $\sin[\frac{1}{2}\theta_{N-1} - (\theta_{N-2} - \frac{1}{2}\theta_{N-3})]$, and $\sin(\frac{1}{2}\theta_{N-1} - \frac{1}{2}\theta_{N-2})$. The first one produces a higher harmonic term $\cos[\frac{3}{2}\theta_{N-1} - \frac{1}{2}(\theta_1 + \theta_N + \theta_{N-2})]$, which cannot be eliminated by the other terms. Thus, the resultant function may vanish only at isolated θ_{N-1}, which implies D_{N-2} can vanish only on some surface in the phase space.

This concludes the proof that there are $N-2$ independent constants of motion out of (B.7). □

B.4. Dependent constants

This section points out some explicit relationships among dependent constants of motion. As shown above, one of the diagonal elements D_{N-1} always vanishes. Accordingly, there must be one dependence relation among $I_1,\ldots,I_{N-1}$.

When $N=4$, there are $(4-1)!/2=3$ constants of motion, i.e. $I_1=\langle 1,2,3,4\rangle$, $I_2=\langle 1,3,4,2\rangle$ and $I_3=\langle 1,4,2,3\rangle$. As Swift found, there is a simpler set of constants of motion, $J_1=S_{12}S_{34}$, $J_2=S_{13}S_{24}$ and $J_3=S_{14}S_{23}$. These sets are related to each other via ${J_1}^2=-I_1I_2/I_3$, ${J_2}^2=-I_2I_3/I_1$ and ${J_3}^2=-I_3I_1/I_2$. Such a reduction of constants of motion is possible for even N. $J_1,\ldots,J_3$ are found to satisfy $J_1+J_3=J_2$. By eliminating $J_1,\ldots,J_3$, and factoring, we obtain the relation in terms of $I_1,\ldots,I_3$ as well:

$$I_1I_2+I_2I_3+I_3I_1=0.$$

For $N>4$, permutation of indices produces more constants of motion than the ones shown in (B.7). When $N=5$, for instance, there are $(5-1)!/2=12$ constants of motion of the form (B.6), i.e. $I_1=\langle 1,2,3,4,5\rangle$, $I_2=\langle 1,3,4,5,2\rangle$, $I_3=\langle 1,4,5,2,3\rangle$, $I_4=\langle 1,5,2,3,4\rangle$, $I_5=\langle 1,2,4,5,3\rangle$, $I_6=\langle 1,4,5,3,2\rangle$, $I_7=\langle 1,5,3,2,4\rangle$, $I_8=\langle 1,3,2,4,5\rangle$, $I_9=\langle 1,2,5,3,4\rangle$, $I_{10}=\langle 1,5,3,4,2\rangle$, $I_{11}=\langle 1,3,4,2,5\rangle$ and $I_{12}=\langle 1,4,2,5,3\rangle$. Three constants of motion out of $I_1,\ldots,I_4$ are independent as proved. The "trivial" relations among $I_1,\ldots,I_{12}$ are:

$$I_1I_{12}=-I_2I_7=-I_3I_{10}=I_4I_5=-I_6I_{11}=I_8I_9,$$
$$I_1I_3I_5=-I_2I_6I_8 \quad\text{and}\quad I_1-I_6=-I_2+I_5=I_3-I_8.$$

These determine $I_5,\ldots,I_{12}$ once $I_1,\ldots,I_4$ are given. The last remaining relation is analogous to the one for $N=4$, namely

$$I_1I_2I_3+I_2I_3I_4+I_3I_4I_1+I_4I_1I_2=0.$$

B.5. Relating the two sets of constants

Now we relate the constants $\{\psi_j\}$ and $\mathcal{H}$ found in Section 4, to the I's shown in (B.7). Consider I_1 of (B.7):

$$\begin{aligned} I_1&=\langle 1,2,3,4,\ldots,N-2,N-1,N\rangle \\ &=\sin[\tfrac{1}{2}(\theta_1-\theta_2)]\sin[\tfrac{1}{2}(\theta_2-\theta_3)]\ldots\sin[\tfrac{1}{2}(\theta_N-\theta_1)]. \end{aligned}$$

The first term of the product is

$$\begin{aligned} \sin[\tfrac{1}{2}(\theta_1-\theta_2)]&=\sin[\tfrac{1}{2}(\theta_1-\Theta)-\tfrac{1}{2}(\theta_2-\Theta)] \\ &=\sin[\tfrac{1}{2}(\theta_1-\Theta)]\cos[\tfrac{1}{2}(\theta_2-\Theta)]-\cos[\tfrac{1}{2}(\theta_1-\Theta)]\sin[\tfrac{1}{2}(\theta_2-\Theta)]. \end{aligned}$$

The half-angle formula corresponding to (3.3) is

$$\sin[\tfrac{1}{2}(\theta_j-\Theta)]=\sqrt{\frac{1+\gamma}{1-\gamma\cos(\psi_j-\Psi)}}\sin[\tfrac{1}{2}(\psi_j-\Psi)],$$

$$\cos[\tfrac{1}{2}(\theta_j - \Theta)] = \sqrt{\frac{1-\gamma}{1-\gamma\cos(\psi_j - \Psi)}}\cos[\tfrac{1}{2}(\psi_j - \Psi)].$$

Thus,

$$\begin{aligned}
&\sin[\tfrac{1}{2}(\theta_1 - \theta_2)] \\
&= \frac{\sqrt{1-\gamma^2}\{\sin[\tfrac{1}{2}(\psi_1 - \Psi)]\cos[\tfrac{1}{2}(\psi_2 - \Psi)] - \cos[\tfrac{1}{2}(\psi_1 - \Psi)]\sin[\tfrac{1}{2}(\psi_2 - \Psi)]\}}{\{[1-\gamma\cos(\psi_1 - \Psi)][1-\gamma\cos(\psi_2 - \Psi)]\}^{1/2}} \\
&= \frac{\sqrt{1-\gamma^2}}{\{[1-\gamma\cos(\psi_1 - \Psi)][1-\gamma\cos(\psi_2 - \Psi)]\}^{1/2}}\sin[\tfrac{1}{2}(\psi_1 - \psi_2)].
\end{aligned}$$

Expressing the other terms similarly, we obtain

$$I_1 = \prod_{k=1}^{N}\frac{\sqrt{1-\gamma^2}}{1-\gamma\cos(\psi_k - \Psi)}\sin[\tfrac{1}{2}(\psi_k - \psi_{k+1})],$$

where indices are reduced mod N. Hence,

$$\frac{1}{N}\log I_1 = \frac{1}{N}\sum_{k=1}^{N}\log(\sin[\tfrac{1}{2}(\psi_k - \psi_{k+1})]) - \frac{1}{N}\sum_{k=1}^{N}\log\left(\frac{1-\gamma\cos(\psi_k - \Psi)}{\sqrt{1-\gamma^2}}\right).$$

From (4.5),

$$\frac{1}{N}\log I_1 = \frac{1}{N}\sum_{k=1}^{N}\log(\sin[\tfrac{1}{2}(\psi_k - \psi_{k+1})]) - \mathcal{H}.$$

This connects I_1 with $\{\psi_j\}$ and $\mathcal{H}$. For the other I's, it is clear from this derivation that only the order of summation in the first term of the right hand side is modified. In particular, if the permutation $(p_1, p_2, \cdots, p_N)$ gives a constant I, then the relation reads:

$$\frac{1}{N}\log I = \frac{1}{N}\sum_{k=1}^{N}\log(\sin[\tfrac{1}{2}(\psi_{p_k} - \psi_{p_{k+1}})]) - \mathcal{H}.$$

References

[1] E. Fermi, J. Pasta and S. Ulam, Los Alamos Rpt. LA-1940 (1955), in: Collected Papers of Enrico Fermi, vol.II (Univ. of Chicago Pr., Chicago, 1965) p. 978.
[2] K. Y. Tsang and I. B. Schwartz, Phys. Rev. Lett. 68 (1992) 2265.
[3] S. Nichols and K. Wiesenfeld, Phys. Rev. A 45 (1992) 8430.
[4] J. W. Swift, S. H. Strogatz and K. Wiesenfeld, Physica D 55 (1992) 239.
[5] D. Golomb, D. Hansel, B. Shraiman and H. Somopolinsky, Phys. Rev. A 45 (1992) 3516.
[6] S. H. Strogatz and R. E. Mirollo, Phys. Rev. E 47 (1993) 220.
[7] K.Y. Tsang, R.E. Mirollo, S.H. Strogatz and K. Wiesenfeld, Physica D 48 (1991) 102.
[8] S. Watanabe and S. H. Strogatz, Phys. Rev. Lett. 70 (1993) 2391.
[9] T. van Duzer and C.W. Turner, Principles of Superconductive Devices and Circuits (Elsevier, New York, 1981).
[10] T.P. Orlando and K.A. Delin, Foundations of Applied Superconductivity (Addison-Wesley, Reading, 1991).
[11] K.K. Likharev, Dynamics of Josephson Junctions and Circuits (Gordon and Breach, New York, 1986).
[12] W.C. Stewart, Appl. Phys. Lett. 12 (1968) 277.
[13] D.E. McCumber, J. Appl. Phys. 39 (1968) 3113.

[14] D.G. Aronson, M. Golubitsky and J. Mallet-Paret, Nonlinearity 4 (1991) 903.
[15] A.K. Jain, K.K. Likharev, J.E. Lukens and J.E. Sauvageau, Phys. Rep. 109 (1984) 310.
[16] J. Bindslev Hansen and P.E. Lindelof, Rev. Mod. Phys. 56 (1984) 431.
[17] R. Kleiner, F. Steinmeyer, G. Kunkel and P. Müller, Phys. Rev. Lett. 68 (1992) 2394; C. Pegrum, Nature 358 (1992) 193.
[18] P. Hadley and M.R. Beasley, Appl. Phys. Lett. 50 (1987) 621.
[19] P. Hadley, M.R. Beasley and K. Wiesenfeld, Phys. Rev. B 38 (1988) 8712.
[20] S.P. Benz and C.J. Burroughs, Supercond. Sci. Tech. 4 (1991) 561; Appl. Phys. Lett. 58 (1991) 2162.
[21] P. Ashwin, J.W. Swift, J. Nonlin. Sci. 2 (1992) 69.
[22] R.E. Mirollo, SIAM J. Math. Anal., in press.
[23] K. Otsuka, Phys. Rev. Lett. 67 (1991) 1090.
[24] J.W. Swift, unpublished.
[25] See e.g. L.G. Taff, Celestial Mechanics (Wiley, New York, 1985).
[26] D. Golomb, personal communication.
[27] M. Tabor, Chaos and Integrability in Nonlinear Dynamics (Wiley, New York, 1989).
[28] A.J. Lichtenberg and M.A. Lieberman, Regular and Stochastic Motion (Springer, New York, 1983).
[29] V.I. Arnold, ed., Dynamical Systems III, Encyclopedia of Mathematical Sciences, vol. 3 (Springer, Berlin, 1988).
[30] M. Hénon and C. Heiles, Astron. J. 69 (1964) 73.
[31] M.B. Sevryuk, Chaos 1 (1991) 160; 3 (1993) 211.
[32] J.W. Swift, to be published.
[33] Y. Yamaguchi, K. Kometani and H. Shimizu, J. Stat. Phys. 26 (1981) 719.
[34] N. Nakagawa and Y. Kuramoto, Prog. Theor. Phys. 89 (1993) 313.
[35] D.W. Jordan and P. Smith, Nonlinear Ordinary Differential Equations (Oxford Univ. Press, New York, 1977).
[36] P. Ashwin, G.P. King and J.W. Swift, Nonlinearity 3 (1990) 585.
[37] M. Toda, Theory of Nonlinear Lattices, 2nd Ed. (Springer, Berlin, 1988); Nonlinear Waves and Solitons (Kluwer, Dordrecht, 1989).
[38] C.J. Goebel, to be published.
[39] H. Flaschka, Phys. Rev. B 9 (1974) 1924.
[40] M. Hénon, Phys. Rev. B 9 (1974) 1921.
[41] J.W. Swift, unpublished.
[42] S. Watanabe, unpublished.